Geological Magazine

www.cambridge.org/geo

Modelling the partial melting of metasediments in a low-pressure regional contact aureole: the effect of water and whole-rock composition

Wei-(RZ) Wang[1,2,3,*], Geoffrey Clarke[2], Nathan R. Daczko[4] and Yue Zhao[1]

[1]Institute of Geomechanics, Chinese Academy of Geosciences, Beijing 100081, China; [2]School of Geosciences, F09, University of Sydney, Sydney, NSW 2006, Australia; [3]State Key Laboratory of Lithospheric Evolution, Institute of Geology and Geophysics, Chinese Academy of Sciences, Beijing 100029, China and [4]GEMOC ARC National Key Centre, Department of Earth and Planetary Sciences, Macquarie University, NSW 2109, Australia

Original Article

Cite this article: Wang W(RZ), Clarke G, Daczko NR, and Zhao Y. (2019) Modelling the partial melting of metasediments in a low-pressure regional contact aureole: the effect of water and whole-rock composition. *Geological Magazine* **156**: 1400–1424. doi:10.1017/S001675681800078X

Received: 7 July 2018
Revised: 6 October 2018
Accepted: 17 October 2018
First published online: 3 December 2018

Keywords:
melt productivity and composition; water content; residuum; migmatite

Author for correspondence:
Wei-(RZ) Wang,
Email: wangwei0521@gmail.com

Abstract

Low-pressure regional aureoles with steep metamorphic field gradients are critical to understanding progressive metamorphism in high-temperature metasedimentary rocks. Delicately layered pelitic and psammitic metasedimentary rocks at Mt Stafford, central Australia, record a greenschist- to granulite-facies Palaeoproterozoic regional aureole, associated with S-type granite plutons, reflecting metamorphism in the range 500–800 °C and at ~3 kbar. The rocks experienced minimal deformation during metamorphism and partial melting. Partial melting textures evolve progressively along the steep metamorphic field gradient from the incipient stages of melting marked by cuspate grains with low dihedral angles, to melt proportions sufficient to form diatexite with schollen. Phase equilibria modelling in the NCKFMASHTO system for pelitic, semi-pelitic and high- and low- ferromagnesian psammitic samples quantitatively illustrates the dependence of partial melting on rock composition and water volume. Pelitic compositions are more fertile than psammitic compositions when the water content in the rocks is low, especially during the early stages of melting. The whole-rock ferromagnesian component additionally influences melt fertility, with ferromagnesian-rich psammite being more fertile than psammite with a lower ferromagnesian component. Subtle variations in free water content can result in obvious changes in melt volume but limited variation in melt composition. Distinct melting histories of pelitic and psammitic rocks inferred from field relationships may be partially attributed to potential differences in water volume retained to supersolidus conditions. Melt composition is more dependent on the rock composition than the variation in water content.

1. Introduction

Regional contact metamorphism has been related to hot intrusions at different crustal levels (e.g. Clarke *et al.* 2010; Craven *et al.* 2012) and commonly exhibits short-lived steep temperature gradients in metasedimentary rocks (White *et al.* 1974; Vernon *et al.* 1990; Collins & Vernon, 1992). These rocks provide opportunities to examine the progressive evolution of rocks with different compositions in the same geological setting. Sedimentary rocks of pelitic (aluminium and ferromagnesian rich), semi-pelitic and psammitic (silica rich and aluminium and ferromagnesian poor) compositions experience partial melting at upper-amphibolite to granulite-facies conditions, and silicate liquid produced from such partial melting may segregate and migrate to be a constituent of common granitic bodies (Fyfe, 1973; Wells, 1981; Powell, 1983; Ben Othman *et al.* 1984; Brown, 1994; Brown *et al.* 1995; White & Powell, 2002; Yardley, 2009).The importance of volatile constituents in the genesis of silicate liquid has been widely acknowledged (Tuttle & Bowen, 1958; Weinberg & Hasalová, 2015), the presence of water facilitating partial melting at far lower temperatures than for otherwise equivalent anhydrous compositions (Johannes & Holtz, 1990). However, if reactant water comes only from that trapped in porosity or loosely bound to crystal faces at high-grade conditions, the volume of water will be very small (Etheridge *et al.* 1984; Clemens & Vielzeuf, 1987). A prediction consequent to this premise is that only a small proportion of silicate liquid will evolve from H_2O-saturated partial melting, in the absence of water ingress (Thompson & Connolly, 1995; Yardley & Valley, 1997, 2000; White *et al.* 2001; Yakymchuk & Brown, 2014). A related prediction is that H_2O-present melting will rapidly evolve to H_2O-absent conditions (Clemens & Vielzeuf, 1987), and melting will continue via the breakdown of hydrous minerals (White *et al.* 2001; Clemens, 2006; Brown & Korhonen, 2009; Brown, 2013). Though partial melting has been mostly considered in terms of either purely fluid-present conditions (e.g. Wickham, 1987; Yardley & Barber, 1991; Holness & Clemens, 1999; Ward *et al.* 2008) or purely fluid-absent conditions (e.g. Braun *et al.* 1996; Kalt *et al.* 1999; Scrimgeour *et al.* 2001; Droop *et al.* 2003), hybrid behaviour may also occur (e.g. White *et al.* 2005; Buick *et al.* 2004; Droop & Brodie, 2012). Minor variations in free water

CAMBRIDGE UNIVERSITY PRESS

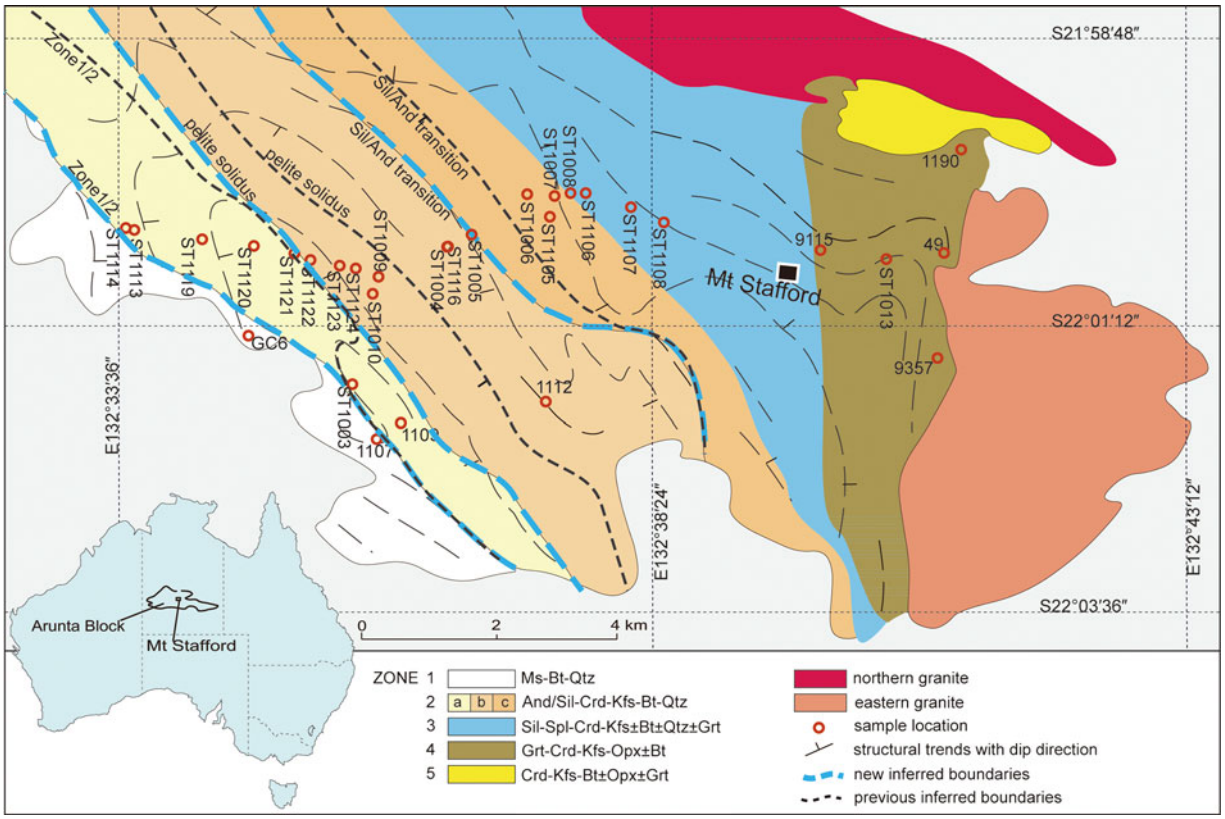

Fig. 1. (Colour online) Geological map of Mt Stafford showing the zone boundaries and sample locations. Representative mineral assemblages for zones from low to high grades are shown in the figure (modified after Greenfield *et al.* 1996, 1998; Wang *et al.* 2014a).

can result in a non-negligible impact on melt productivity and composition during partial melting along a given thermal gradient (Holtz & Johannes, 1991; Stevens *et al.* 1997; Droop & Brodie, 2012; Weinberg & Hasalová, 2015).

A low-pressure greenschist- to granulite-facies regional aureole of *c.* 10 km width occurs at Mount Stafford, in the central Australian Arunta Block (Fig. 1) (Vernon *et al.* 1990; Greenfield *et al.* 1996, 1998; White *et al.* 2003). Migmatite exposures at Mt Stafford preserve a sequence of metamorphic isograds and provide the opportunity to investigate the partial melting evolution in a suite of common metasedimentary rocks. In particular, metapelitic and metapsammitic layers of 'bedded migmatite' (Greenfield *et al.* 1996) have distinct melting histories, apparently as a consequence of subtle changes in bulk composition. Metapelitic layers are interpreted as recording extensive partial melting, whereas metapsammitic layers are mostly inferred to have experienced less extensive melting (Greenfield *et al.* 1996). Building on previous work on the mineral assemblage and textural development (Greenfield *et al.* 1996; White *et al.* 2003), we investigate: (1) the dependence of melt composition and productivity on the bulk protolith composition and water content of metasedimentary rocks; and (2) the compositional consequence of melt loss from common metasedimentary rocks by integrating petrographical and compositional analyses with the results of phase equilibria modelling.

2. Geological setting

Mt Stafford occurs at the northwestern end of the Anmatjira–Reynolds Range, in the Arunta Block, central Australia (Noakes, 1953; Stewart, 1981). The Arunta Block is characterized by extensively deformed, low- to high-grade Proterozoic metasedimentary rocks and orthogneiss (Warren, 1983; Stewart *et al.* 1984). The Mt Stafford area is dominated by metamorphosed turbidites of the Lander Rock Beds, previously inferred to have been deposited at *c.* 1870 Ma and metamorphosed at *c.* 1800 Ma (Blake & Page, 1988; Clarke *et al.* 1990; Compston, 1995). However, detrital zircons from the Lander Rock Beds as young as 1838 Ma (Vry *et al.* 1996) and 1820 Ma (Rubatto *et al.* 2006) indicate that the deposition probably occurred shortly before the *c.* 1800 Ma metamorphic event (Rubatto *et al.* 2006).

Delicately interbedded metapelite and metapsammite at Mt Stafford have well-preserved sedimentary structures and are inferred to be components of a turbidite sequence (Stewart *et al.* 1984). Layered rocks dominate outcrop throughout the transition from greenschist- to granulite-facies assemblages, leading to the term 'bedded migmatite' in the high-grade rocks (Greenfield *et al.* 1996). The area is unusual for its excellent preservation and exposure of a high-temperature–low-pressure (HT–LP) regional contact aureole (after Hanson & Barton, 1989). There are only minimal effects of deformation through the regional aureole such that many rocks retain a hornfels texture (Stewart *et al.* 1984).

The regional aureole at Mt Stafford has been divided into five zones (Vernon *et al.* 1990; Greenfield *et al.* 1996; Fig. 1). The rocks of Zone 1 comprise poorly exposed schist dominated by muscovite, biotite and quartz, with or without cordierite and andalusite (Vernon *et al.* 1990). The transition to Zone 2 is marked by the sub-solidus breakdown of muscovite to andalusite and K-feldspar (Vernon *et al.* 1990), with subdivisions of the higher-grade parts of Zone 2 based on the first occurrence of metatexite in metapelitic

https://doi.org/10.1017/S001675681800078X Published online by Cambridge University Press

rocks (Zone 2b) and then the first occurrence of prismatic sillimanite (Zone 2c; Greenfield *et al.* 1996). The first metatexite was inferred by Greenfield *et al.* (1996) to reflect the onset of water-present partial melting. The lower limit of Zone 3 is defined by the appearance of hercynitic spinel, mostly in intergrowths with cordierite that mantles aluminosilicate. This boundary is accompanied by a marked reduction in biotite mode in all rocks. Zone 4 is distinguished by the appearance of mineral assemblages involving garnet, orthopyroxene and cordierite in metapsammitic rocks (Greenfield *et al.* 1996, 1998). Zone 5 includes hybrid diatexite, inferred by Greenfield *et al.* (1996) to have formed through the injection of granitic magma into high-grade migmatite. Considering the role of whole-rock composition on partial melting, the boundaries of the Zone 2 subdivisions and the Zone 2–3 boundary should reflect a series of high variance reactions between biotite and aluminosilicate and should not be considered as isograds (White *et al.* 2003). The proposed zonal divisions did not evaluate the effects of changes in whole-rock composition, or account for the development of distinct compositional domains within rocks (White *et al.* 2003). Nonetheless, they generally reflect a sequence of reactions controlling the greenschist–granulite transition and are used as a convenient spatial and grade framework in this paper.

3. Melting development in the field

Partial melting initiated in the low-grade zones at Mt Stafford. It is seldom straightforward to infer the former presence of silicate liquid in rocks that experienced small degrees of partial melting, and hence identify the true position of solidi in field settings. The grain-scale distribution of liquid in melt-poor crustal rocks is commonly inferred from the presence of cuspate or poikilitic grains with boundaries defining low dihedral angles (e.g. Harte *et al.* 1991; Holness & Clemens, 1999; Holness & Sawyer, 2008; Holness *et al.* 2011; Wang *et al.* 2014*b*; Stuart *et al.* 2016, 2017). Such grains are indicative of the former presence of melt and have been termed interserts (Rosenberg & Riller, 2000), pseudomorphs after melt (Marchildon & Brown, 2002) or melt pseudomorphs (e.g. Harte *et al.* 1993; Clemens & Holness, 2000; Brown, 2001; Walte *et al.* 2005). Delicate mineral films overgrowing grains and quartz blebs occurring as intergrowths between grains have also been used to infer the former presence of melt (e.g. Guilmette *et al.* 2011). Metasedimentary rocks formed in the lower temperature zones at Mt Stafford preserve delicate textures from partial melting that are described in detail below.

Intermittent centimetre-scale lenticular leucosome oriented predominantly normal to bedding in the Zone 2b metapelitic layers of 'bedded migmatite' were used by Greenfield *et al.* (1996) to mark the inferred change to supra-solidus conditions for that rock type. Some transgressive leucocratic segregations in this zone contain euhedral andalusite, consistent with partial melting having initiated in the andalusite field. Large grains of K-feldspar in such segregations commonly have inclusion-rich cores and clear idioblastic rims sometimes mantled by plagioclase (Greenfield *et al.* 1998). In general, leucosome development becomes more extensive as grade increases through and above Zone 2b. Schlieren migmatite (after Mehnert, 1968) and migmatite with well-developed melanosome and mesosome first appears in Zone 3 rocks. Melanosome development commonly occurs at the compositional boundary of psammitic and pelitic portions of bedded migmatite (Greenfield *et al.* 1998; Wang *et al.* 2014*a*). Nebulitic leucosome may compose up to 20% (by volume) of the metapelite layers, commonly centred on aluminosilicate aggregates and forming extensive vein networks (fig. 2c in Greenfield *et al.* 1998). Though Zone 4 metapelitic layers contain abundant diatexite (after Brown, 1973), interlayered metapsammite also preserves sedimentary features reflecting low strain and restricted melting in the psammitic layers (Vernon *et al.* 1990; Greenfield *et al.* 1996).

4. Petrology at the early stage of partial melting

Samples were collected on an E-trending section (Fig. 1) along Spring Creek, further west than exposures used in the previous detailed studies that mainly focused on high-grade partial melting (e.g. Greenfield *et al.* 1996). Samples representative of the early stage of partial melting are described in detail from the lower temperature side (west) to the higher temperature side (east). Interlayered (semi-) pelitic and psammitic rocks at sites ST1113, ST1114, ST1119 and ST1120 fall in the Zone 1 inferred by Greenfield *et al.* (1996). However, here we show that their mineral assemblages and textures are consistent with those being part of Zone 2 (Fig. 1). The rocks mostly have a hornfelsic texture defined by random aggregates of biotite, retrogressed cordierite and, in pelitic layers, andalusite in a felsic matrix. Some thin semi-pelitic layers retain a weak biotite foliation (S1), oriented sub-parallel to compositional layering. Pelitic layers consist of andalusite, biotite, muscovite, K-feldspar and quartz with minor plagioclase, tourmaline (~5%) and ilmenite. Andalusite commonly occurs as larger poikiloblasts with abundant inclusions of K-feldspar and quartz. Symplectites of biotite and fine-grained (commonly <0.2 mm) andalusite are inferred to pseudomorph cordierite. K-feldspar has inclusions of quartz, muscovite and rare biotite. Rare plagioclase occurs as inclusions in K-feldspar. Muscovite is heterogeneously distributed, occurring mostly along compositional boundaries between pelitic and semi-pelitic layers. Minerals forming semi-pelite are smaller (<0.2 mm) than in adjacent pelitic schist. Assemblages involve biotite, andalusite, K-feldspar and quartz with accessory tourmaline and ilmenite. Andalusite grains are smaller (~0.1 mm) and occur in lower modes (~7%) than in equivalent pelitic layers. Biotite–andalusite symplectite partially (ST1120) to completely (ST1119) pseudomorphs cordierite. The average grain size in the semi-pelitic schist increases subtly with grade, from ~0.2 mm at site ST1119 to ~0.3 mm at ST1120 (Fig. 1). Large, clear grains of quartz (~0.5 mm) may be of sedimentary origin. Psammitic sample ST1120B contains a mineral assemblage similar to the semi-pelitic sample at that site but has more felsic components. The paired semi-pelite 1107spe and psammite 1107ps samples were collected from the Zone 1–2 boundary (JE Greenfield, unpub. Ph.D. thesis, Univ. Sydney, 1997; White *et al.* 2003).

Pelitic schist at site ST1121 (Figs 1, 2a) consists of andalusite, biotite, cordierite, K-feldspar, plagioclase and quartz with accessory tourmaline and ilmenite. Abundant symplectite of biotite and andalusite has mostly pseudomorphed cordierite. Some andalusite grains occur as large poikiloblasts. Polygonal cordierite and K-feldspar commonly have abundant inclusions of quartz and (pre-symplectic) biotite, but examples of both also occur with few inclusions. Quartz in low modes occurs as grains of cuspate form and develops web-style textures enclosing biotite (Fig. 3a), consistent with the former presence of melt. Semi-pelitic schist at this site is similar in assemblage and texture, but has less biotite and lacks andalusite. Metapsammitic schist at this site (e.g. bottom layer in Fig. 2a) comprises biotite, K-feldspar, andalusite, muscovite, plagioclase, quartz and accessory ilmenite. It has less biotite

https://doi.org/10.1017/S001675681800078X Published online by Cambridge University Press

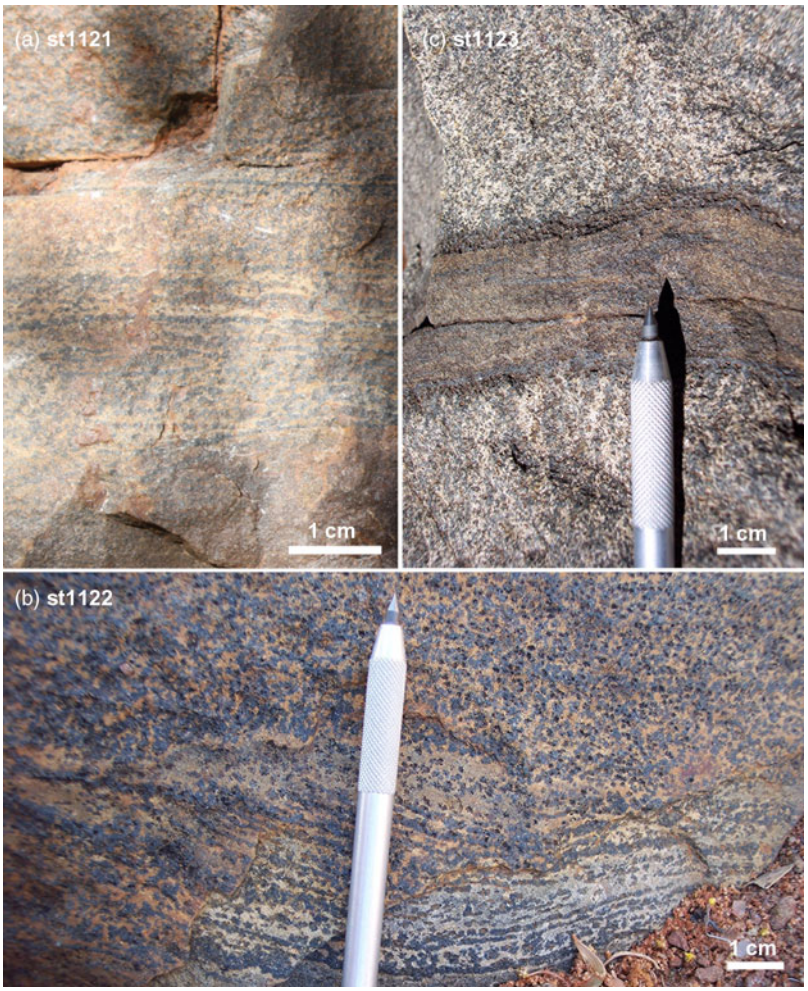

Fig. 2. (Colour online) Field photographs. (a) Interbedded metapelite (middle and upper) and metapsammite (bottom) from location ST1121, original sedimentary layering being well preserved in the metapelite. (b) Metapelite sample with sedimentary bedding from location ST1122. (c) Interbedded metapelite (bottom and upper) and metapsammite (middle) from location ST1123, with metapelite layer showing nebulitic patches of leucosome and dark selvage developing between metapelite and metapsammite.

(<10%) and much more quartz (>50%) than the pelitic schist at the site. Symplectite of biotite and andalusite is common. Quartz is granular and some grains almost equant; as samples lack cuspate grain shapes they are inferred to have remained at sub-solidus conditions in distinction to adjacent pelitic schists. Muscovite, in low proportions, partially replaces biotite.

Grade increases in the upper part of Zone 2a continue to be marked by subtle grain coarsening. The average grain size in pelitic schist at site ST1122 (Fig. 2b) is ~0.5 mm. Andalusite occurs as both large (~2 mm) poikiloblasts and small grains in the metapelitic schist. Cordierite occurs as smaller equant grains, extensively pseudomorphed by biotite–andalusite symplectite. Subhedral K-feldspar (microcline) has abundant quartz and biotite inclusions. Features of minerals in the samples suggest the presence of previous melt: quartz interstitial to K-feldspar and cordierite retains cuspate forms (Fig. 3b, c). Film-like quartz also formed around adjacent K-feldspar and/or andalusite (Fig. 3b, c), and occasionally such quartz films were recrystallized to sub-grains in string-of-beads textures (Fig. 3d) (Holness & Clemens, 1999). The transition to metatexite, evident in the field setting (former Zone 2b), occurs at site ST1123 on the Spring Creek section (Fig. 1), where metapelitic layers include nebulitic migmatite with isolated, patch-style leucosome. Compositional layering is well preserved in psammitic layers, but disrupted by recrystallization and melt segregation in pelitic layers. Metapelitic layers (bottom and upper layers in Fig. 2c) comprise andalusite, biotite, K-feldspar, cordierite, plagioclase and quartz with accessory ilmenite and tourmaline. Grain size is ~0.5 mm. Andalusite is subhedral to euhedral. Cordierite is extensively pseudomorphed by symplectite of biotite and andalusite, but some well-preserved grains occur with cores rich in inclusions of quartz and biotite and clear rims. K-feldspar and/or perthite commonly occur as subhedral grains. Plagioclase occurs in low modes. Quartz grains commonly have cuspate grain forms. Metapsammitic layers (middle layer in Fig. 2c) comprise biotite, cordierite, quartz and accessory ilmenite. Only minor K-feldspar and plagioclase can be observed. Grain size is small compared with adjacent pelitic layers (<0.2 mm). The first textures typical of partial melting in psammitic rocks occur at site ST1123 and involve poikiloblastic quartz with cuspate boundaries against biotite or plagioclase (Fig. 3e), quartz with cuspate symmetric necks separating quartz and plagioclase (Fig. 3f, g), and rounded quartz blebs with overgrowths of cuspate quartz (Fig. 3g, h). Striking dark selvages developed between pelitic and psammitic layers in bedded migmatite at site ST1123 and persist throughout the rest of Zone 2 and up to Zone 4. They are richer in biotite, cordierite and ilmenite than their hosts.

Sillimanite is first developed in pelitic rocks at site ST1005, slightly lower than the previously defined sillimanite/andalusite line, marking the transition to Zone 2c (Fig. 1, after Greenfield *et al.* 1996, 1998). The pelitic layers comprise biotite, cordierite, andalusite, K-feldspar, muscovite and tourmaline. Cordierite is partially to completely pseudomorphed by symplectite of biotite

https://doi.org/10.1017/S001675681800078X Published online by Cambridge University Press

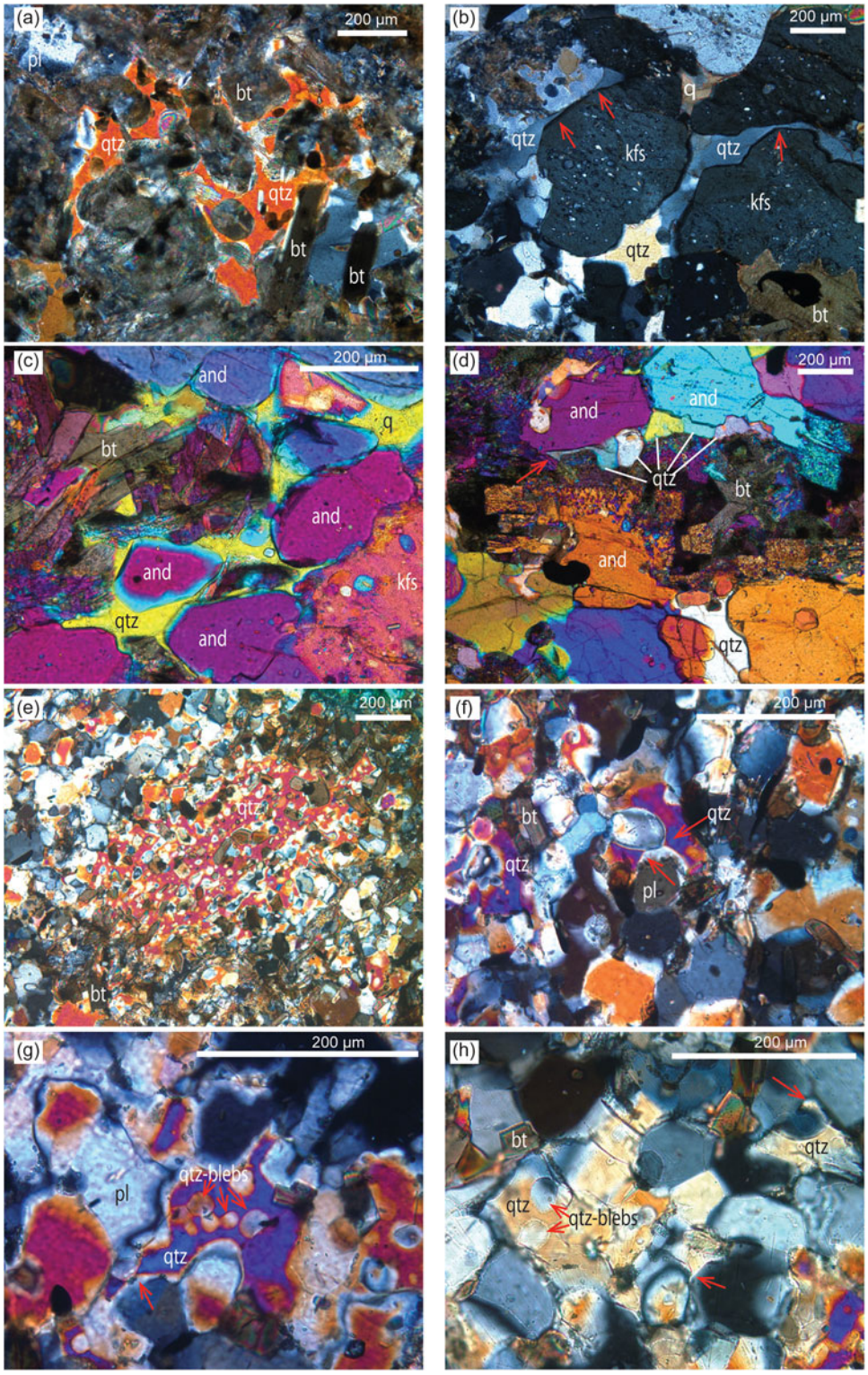

Fig. 3. (Colour online) Photomicrographs showing microstructures indicative of the former presence of melt in metapelite ((a) ST1221, (b–d) ST1122) and metapsammite ((e–h) ST1123). (a) Optically continuous cuspate quartz (qtz) developing web-style textures enclosing biotite (bt), implying a former melt pool (ST1121). Plane-polarized light. (b) Cuspate quartz with very small dihedral angle of boundaries (two arrows on the left) and quartz film around K-feldspar (kfs) (arrow on the right) (ST1122). Cross-polarized light. (c) Interstitial quartz in cuspate shape among andalusite (and), biotite and K-feldspar (ST1122). Cross-polarized light with gypsum plate. (d) String-of-beads of quartz recrystallized from previous melt. Note the quartz bead on the left with a long neck with sharp points (left arrow) (ST1122). Cross-polarized light with gypsum plate. (e) Poikiloblastic quartz with cuspate boundaries against biotite or plagioclase indicating former melt pool (ST1123). Cross-polarized light with gypsum plate. (f) Quartz with cuspate symmetric necks separating quartz and plagioclase (pl) (ST1123). Cross-polarized light. (g) Interstitial quartz with cuspate edge (left arrow) enclosing smaller rounded quartz blebs (ST1123). Cross-polarized light. (h) Quartz grains with tiny neck into plagioclase (right arrow), a symmetric cuspate edge (middle arrow) as well as small blebs (left arrows) (ST1123). Cross-polarized light.

and andalusite. Andalusite persists as large porphyroblasts, partially pseudomorphed by prismatic sillimanite. Euhedral K-feldspar (microcline) grains retain straight edges against interstitial quartz. Retrograde muscovite occurs along grain boundaries or in corroded cores of K-feldspar grains. Plagioclase is virtually absent. Tourmaline mode can be as high as ~5%. Minerals are mostly larger than in lower grade zones.

5. Whole-rock compositions

Whole-rock compositions of 58 metasedimentary samples from Mt Stafford were determined by XRF (X-ray fluorescence) analysis (online Supplementary Material Table S1). Thirty samples represent new data, and 28 samples were drawn from previous work (JE Greenfield, unpub. Ph.D. thesis, Univ. Sydney, 1997). Data are

https://doi.org/10.1017/S001675681800078X Published online by Cambridge University Press

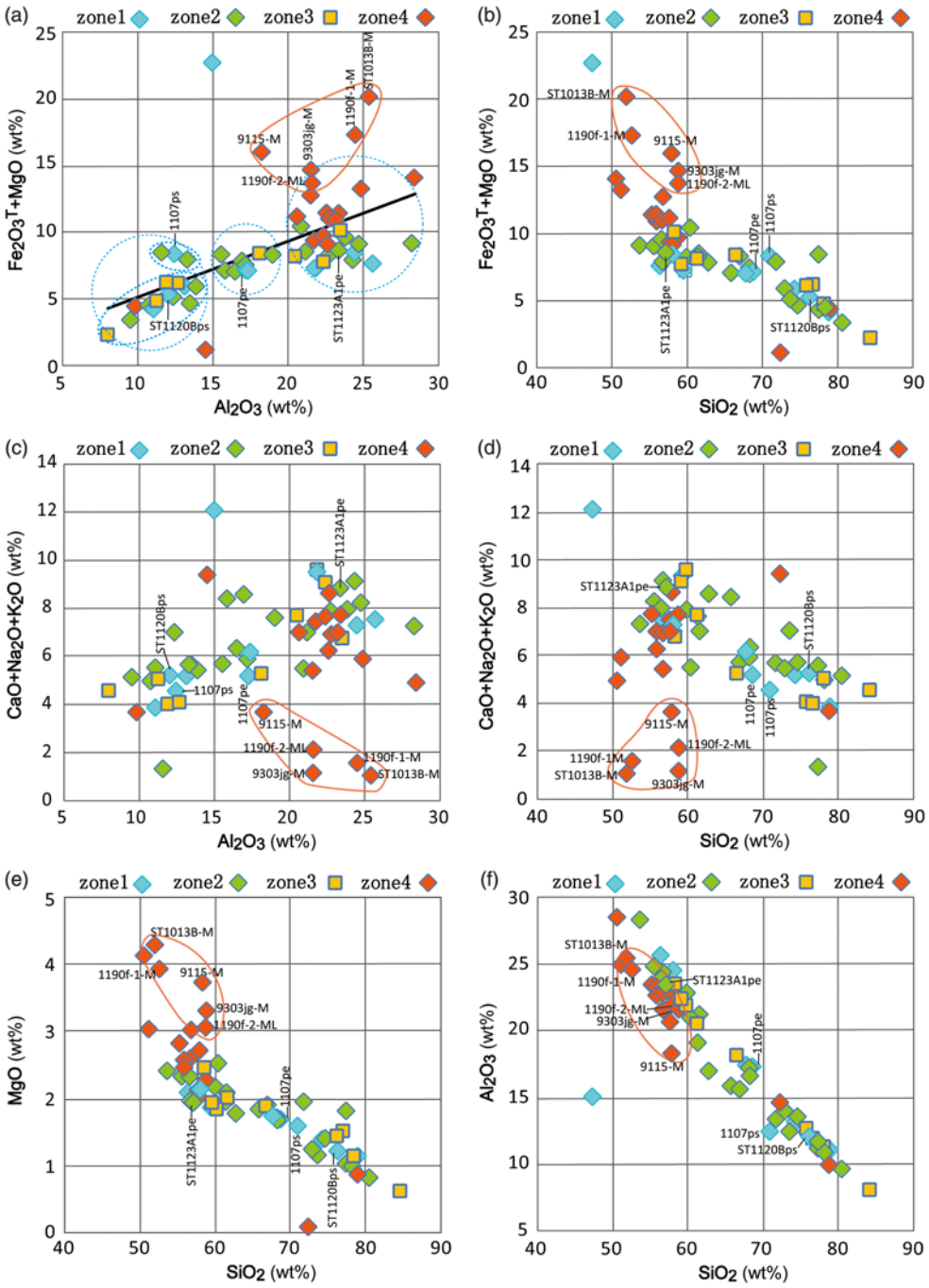

Fig. 4. (Colour online) Binary plots displaying major element variation for the XRF data compiled in online Supplementary Material Table S1.

plotted on a series of diagrams illustrating compositional dependencies both between samples within a given zone and spatially across the four main zones (Fig. 4). In binary diagrams involving alumina or silica content as a variable (e.g. Fig. 4a, f), the whole-rock data generally cluster in three groups, corresponding to the pelitic, semi-pelitic and psammitic compositions identified in the field. There is a general first-order relationship between silica and alumina content, alumina content being highest in pelitic samples and silica content highest in psammitic samples (e.g. Fig. 4f). There are also first-order relationships between: (1) ferromagnesian ($Fe_2O_3^T$ + MgO) and alumina or silica contents (Fig. 4a, b); and (2) total alkali (CaO + Na_2O + K_2O) and alumina contents (Fig. 4c). Breaks in the overall linear trend between pelitic and semi-pelitic rocks, and between semi-pelitic and psammitic rocks (e.g. Fig. 4a) may reflect depositional sorting or a sampling bias. Psammitic samples can be further sub-divided in terms of ferromagnesian content (Fig. 4a), with three samples from zones 1 and 2 having subtly higher ferromagnesian contents and plotting above the general linear trend (Fig. 4a). Some metapelitic layers in the Zone 3 and 4 'bedded migmatite' were referred to as 'mesosome' by Greenfield *et al.* (1996), because a type of melanosome commonly separates psammitic from pelitic and semi-pelitic layers attributing a large-scale leucosome–melanosome–mesosome appearance (terms after Mehnert, 1968). Such pelitic samples (melanosome/mesosome, outlined in red) have elevated ferromagnesian (Fig. 4a, b, e; samples suffixed with M) and depleted total alkali content (Fig. 4c, d), and are distinct from other metapelitic rocks across the regional aureole.

https://doi.org/10.1017/S001675681800078X Published online by Cambridge University Press

Table 1. Bulk rock compositions used in calculations for pseudosections (mol. %). The compositions of 1107spe and 1107ps are after JE Greenfield (unpub. Ph.D. thesis, Univ. Sydney, 1997) and White *et al.* (2003)

Figure	Sample		H_2O	SiO_2	Al_2O_3	CaO	MgO	FeO	K_2O	Na_2O	TiO_2	O
Figure 5a	ST1123A1pe	X = 0	0	66.575	16.058	0.562	3.352	5.838	5.268	1.468	0.588	0.292
		X = 20	20	53.260	12.846	0.449	2.681	4.671	4.215	1.175	0.470	0.234
Figure 5b	1107spe	X = 0	0	76.478	11.310	0.210	2.810	4.552	3.195	0.564	0.469	0.412
		X = 20	20	61.182	9.048	0.168	2.248	3.641	2.556	0.451	0.375	0.329
Figure 5c	1107ps	X = 0	0	79.102	8.198	0.174	2.647	5.668	2.706	0.665	0.421	0.418
		X = 20	20	63.282	6.558	0.139	2.118	4.534	2.165	0.532	0.337	0.334
Figure 5d	ST1120Bps	X = 0	0	82.259	7.667	0.602	1.947	3.299	2.397	1.298	0.366	0.165
		X = 20	20	65.807	6.134	0.482	1.558	2.639	1.918	1.038	0.293	0.132
Figure 10	ST1123A1pe		3.2	64.445	15.544	0.544	3.244	5.651	5.100	1.421	0.569	0.282
	1107spe		2.2	74.796	11.061	0.205	2.748	4.451	3.125	0.552	0.458	0.403
	1107ps		2.7	76.966	7.977	0.169	2.576	5.515	2.633	0.647	0.409	0.406
	ST1120Bps		1.81	80.770	7.528	0.591	1.912	3.239	2.353	1.274	0.359	0.162
Figure 11	ST1123A1pe		4.2	63.779	15.384	0.538	3.211	5.593	5.047	1.406	0.563	0.280
	1107spe		3.2	74.031	10.948	0.203	2.720	4.406	3.093	0.547	0.454	0.399
	1107ps		3.7	76.175	7.895	0.168	2.549	5.458	2.606	0.641	0.405	0.402
	ST1120Bps		2.81	79.947	7.451	0.585	1.893	3.206	2.330	1.261	0.356	0.160

6. Phase equilibria modelling

A series of *T*–*X* and *P*–*T* diagrams were constructed for different metasedimentary rock compositions from the Mt Stafford region in the model system Na_2O–CaO–K_2O–FeO–MgO–Al_2O_3–SiO_2–H_2O–TiO_2–O (Fe_2O_3) (NCKFMASHTO) using the software THERMOCALC (3.33i, Powell *et al.* 1998, updated) with the internally consistent thermodynamic dataset 5.5 of Holland & Powell (1998, updated November 2003). Minerals and activity models used in the construction of the *P*–*T* and *T*–*X* pseudosections are biotite (bt; White *et al.* 2007), garnet (grt; White *et al.* 2007), muscovite (ms; Coggon & Holland, 2002), plagioclase (pl; Holland & Powell, 2003), K-feldspar (kfs; Holland & Powell, 2003), ilmenite (ilm; White *et al.* 2000), spinel (sp; White *et al.* 2002), orthopyroxene (opx; White *et al.* 2002), cordierite (crd; Holland & Powell, 1998), magnetite (mag) for sub-solidus (White *et al.* 2000) and supra-solidus (White *et al.* 2002) conditions, and silicate melt (liq; White *et al.* 2007). Quartz (qtz), sillimanite (sil), andalusite (and) and water (H_2O) were modelled as pure end-member phases. Representative pelitic, semi-pelitic and high- and low-ferromagnesian psammitic rock compositions determined by whole-rock XRF analyses and subsequently converted to molar proportions for the phase equilibria modelling are given in Table 1. The assumption in the ferric–ferrous proportion is 10% of the total iron being ferric (Fe^{3+}), on the basis of mineral chemistry and test modelling to obtain oxide proportions that most closely matched those observed in thin-sections. Samples collected from zones 1 and 2a are taken from rocks that experienced no or insignificant partial melting, and thus give the best available indications of protoliths to the Zone 3 and 4 rocks.

6.a. *T–X diagrams*

The greenschist- to granulite-facies transition at Mt Stafford was accompanied by a minor increase (<1 kbar) in pressure from ~3 kbar (White *et al.* 2003). *T–X(H$_2$O)* pseudosections were constructed in NCKFMASHTO for representative pelitic, semi-pelitic, high- and low-ferromagnesian psammitic compositions at P = 3 kbar for T = 650–900 °C and H_2O = 0–20 mol.% for the purpose of evaluating the dependences of melt fertility on rock composition and water content (Fig. 5). The water content was modelled for the large range 0–20 mol.%, although it is rare for metasedimentary rocks to have extremely low or high water contents (e.g. Yardley, 2009). In the range, the value of the water content in molar per cent corresponds to three to four times that in weight per cent. Molar melt contours are shown as dashed lines in each of the pseudosections. Solidi are highlighted in bold, and equilibria variance is reflected in colour intensity. Equilibria in the *T–X(H$_2$O)* diagrams indicate a general evolution from low to high variance assemblages with increasing temperature and/or increasing water content. The modelling generally reflects well the observed parageneses involving cordierite, K-feldspar, biotite, sillimanite, ilmenite, magnetite, quartz and liquid, with orthopyroxene also occurring in psammitic compositions. Cordierite occurs in most modelled equilibria except for those formed at low-T water-saturated extremes. Biotite-bearing assemblages are predicted for the pelitic composition ST1123A1 (Fig. 5a) at T <~700 °C for low H_2O contents; biotite stability expands at high T for increasing water content. For the modelled semi-pelitic composition (1107spe), biotite stability is predicted to be more restricted and only stable at T < ~700 °C independent of water content (Fig. 5b). Biotite is predicted to have a larger stability range at intermediate and low-T conditions for psammitic compositions (1107ps, ST1120Bps; Fig. 5c, d). It is predicted to breakdown to orthopyroxene at $T \approx 800$ °C in psammitic compositions across a broad range of H_2O contents. Sillimanite is predicted to be present in pelitic and semi-pelitic compositions (Fig. 5a, b) over a wide range of temperature conditions, especially in low H_2O conditions. It is predicted to be restricted to T < 690 °C in psammitic compositions (Fig. 5c, d). K-feldspar and plagioclase are predicted to occur over a wide temperature range for low H_2O content, but progressively break down as H_2O content and T increase. Quartz is predicted to only occur at low water contents in the modelled pelitic compositions (Fig. 5a), but to be stable

https://doi.org/10.1017/S001675681800078X Published online by Cambridge University Press

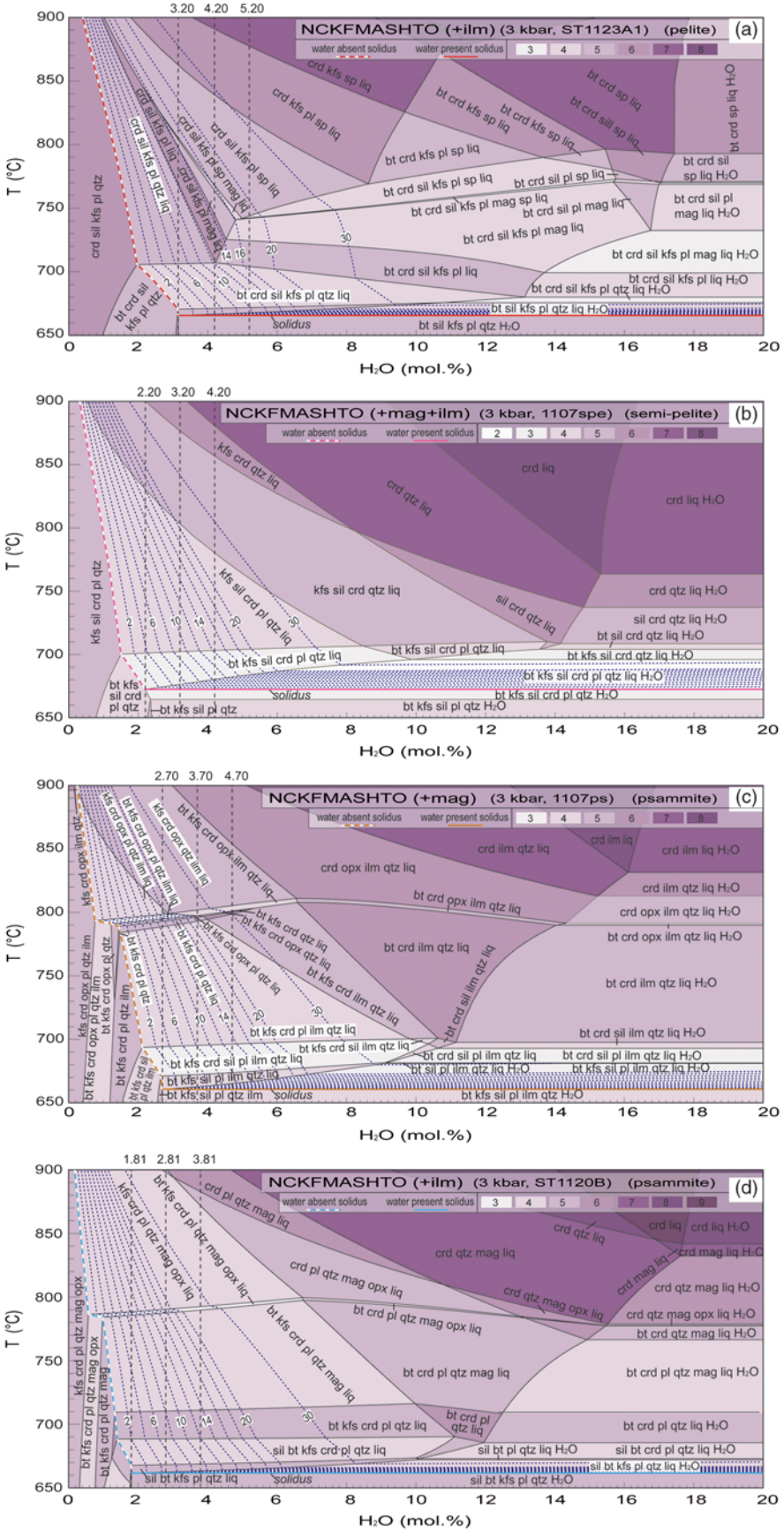

Fig. 5. (Colour online) Calculated *T–X(H$_2$O)* pseudosections for metasedimentary rocks of varying compositions at 3 kbar. The x-axis shows an increase in H_2O content in the system from left to right (mol. %). The value of the water content in molar per cent is approximately three to four times that in weight per cent. Calculated molar mode contours in per cent for melt are shown with dashed lines in each pseudosection. Variance of equilibria in stability fields is indicated in the legend. (a) Pelitic sample ST1123A1. (b) Semi-pelitic sample 1107spe. (c) High-ferromagnesian psammitic sample 1107ps. (d) Psammitic sample ST1120Bps. See the specific compositions used in calculations of the pseudosections in Table 1. The vertical dashed lines in each diagram mark the specific water modes and the evolutionary paths with increasing temperature.

https://doi.org/10.1017/S001675681800078X Published online by Cambridge University Press

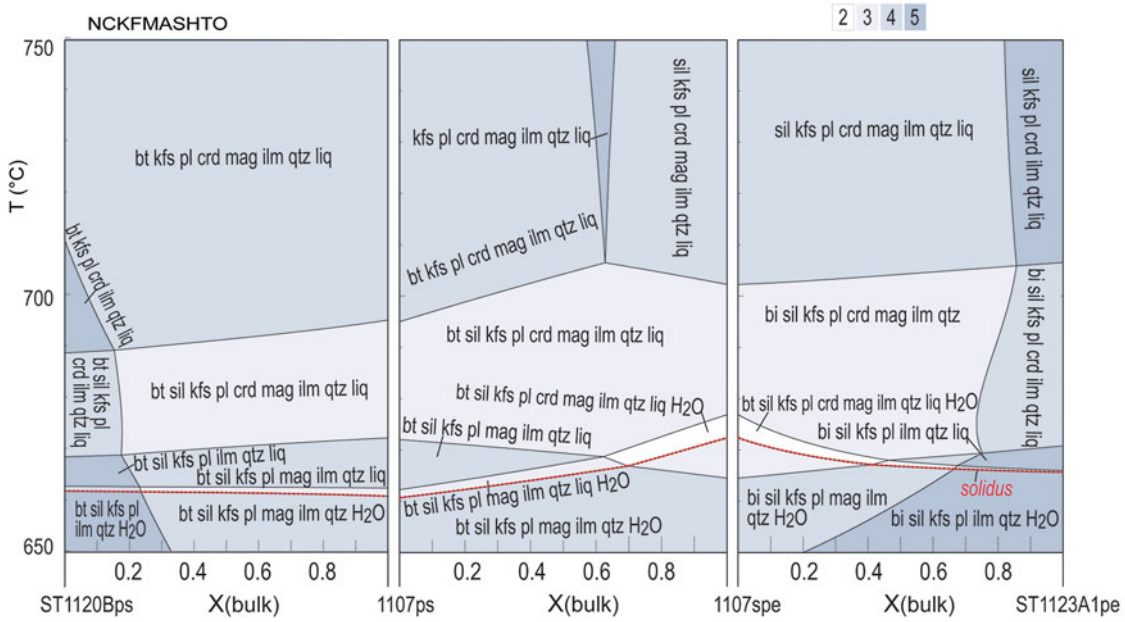

Fig. 6. (Colour online) Calculated *T–X(bulk)* pseudosections based on the four types of compositions used in Figure 5, showing the influence of bulk composition on the solidus. See the compositions used in Table 1. Water contents were set a bit higher to ensure H_2O saturation, which does not affect the water-saturated solidus. The solidus is highlighted by a dotted line at the bottom.

across almost the full range of modelled *X(H$_2$O)* conditions for semi-pelitic and psammitic compositions (Fig. 5b, c, d).

For free-water-absent assemblages, the modelling reflects a general antithetic relationship between solidus *T* and bound-H_2O content. Initial partial melting occurs at the water-saturated solidus if any free water is available. A series of sub-solidus biotite breakdown reactions at $T < 790$ °C in psammitic compositions (Fig. 5c, d), and at $T < 700$ °C in pelitic and semi-pelitic compositions (Fig. 5a, b), result in steps in the free-water-absent solidi (Fig. 5). Sillimanite breakdown coupled with the persistence of biotite in psammitic compositions at $T \approx 690$ °C (Fig. 5c, d) results in a subtle kink in the relevant solidi for water-absent assemblages. The H_2O content required to just saturate low-*T* assemblages varies with ferromagnesian content of the rock composition (Fig. 5a–d; Table 1). For example, the psammitic sample 1107ps with higher ferromagnesian content ($X_{FeO+MgO} \approx 8.02$ wt%) needs ~2.7 mol.% H_2O to become saturated, whereas the semi-pelitic sample 1107spe with lower ferromagnesian content ($X_{FeO+MgO} \approx 7.12$ wt%) needs only ~2.2 mol.%. This is because higher ferromagnesian content increases the modal content of hydrate minerals such as biotite. The high ferromagnesian content tends to retain more bound H_2O to the onset of partial melting, even though the rock has less alumina.

The dependence of solidi temperature on compositional spectra between the samples chosen as representative in the *T–X* diagrams (at fixed *P* and water saturation) is shown in Figure 6. Partial melting is predicted to occur at slightly varying temperatures for different rock compositions; however, the difference in temperature is minimal.

6.b. Modelling melt development at 3 kbar

Melt mode contours (blue dashed lines) on the *T–X(H$_2$O)* pseudosections (Fig. 5a–d) indicate a general increase in melt mode with *T* at a given H_2O content. For water-saturated conditions, melt mode is predicted to reach 30% at *c.* 675 °C, 690 °C, 680 °C and 670 °C for pelitic, semi-pelitic and high- and low-ferromagnesian psammitic compositions, respectively. Limited melting occurred at solidus conditions for all metasedimentary rocks at Mt Stafford, based on petrographic relationships including the excellent preservation of depositional features. These relationships also indicate that there was no significant water ingress; otherwise more extensive partial melting would have occurred. On the other hand, prograde sub-solidus metamorphism and the breakdown of hydrous minerals result in the temperature-dependent liberation of bound water and the possibility of water-saturated conditions persisting to the solidus. The amount of water released at the solidus is dependent on the composition of the metasedimentary rocks. Pelitic compositions commonly have higher muscovite contents and thus have the potential to release higher amounts of water. If the temperature increased rapidly from conditions appropriate for muscovite dehydration to the solidus, it is likely that some released water will be retained in the rocks and consequently effect the extent of partial melting. However, differences in the amount of water released by pelitic and psammitic rocks must be small (e.g. Yardley, 2009). We considered different situations with free water of 0, 1 and 2 mol.% at the solidus of the pelitic and psammitic rocks. Melt productivity as a function of temperature, and assuming no melt loss or gain, for the four compositions with various water contents were modelled and compiled in Figure 7.

With low water content (free $H_2O = 0$), the pelitic and semi-pelitic compositions are predicted to have a relatively steep slope of the *T* versus melt fraction from the solidus to ~700 °C, and then the slope becomes gentle as a consequence of the exhaustion of biotite (Fig. 7a–e). Isopleths of melt mode retain a consistent gradient for heating at fixed water content to the maximum modelled *T* of 900 °C, but the isopleths become more closely spaced at elevated temperatures (Fig. 5a, b) as the melt becomes progressively drier (e.g. Johannes & Holtz, 1996). The slope of the *T* versus melt fraction for psammitic compositions is predicted to be gentler than those for either pelitic or semi-pelitic compositions (Fig. 7a–e), but it becomes much steeper from ~800 °C when the breakdown

https://doi.org/10.1017/S001675681800078X Published online by Cambridge University Press

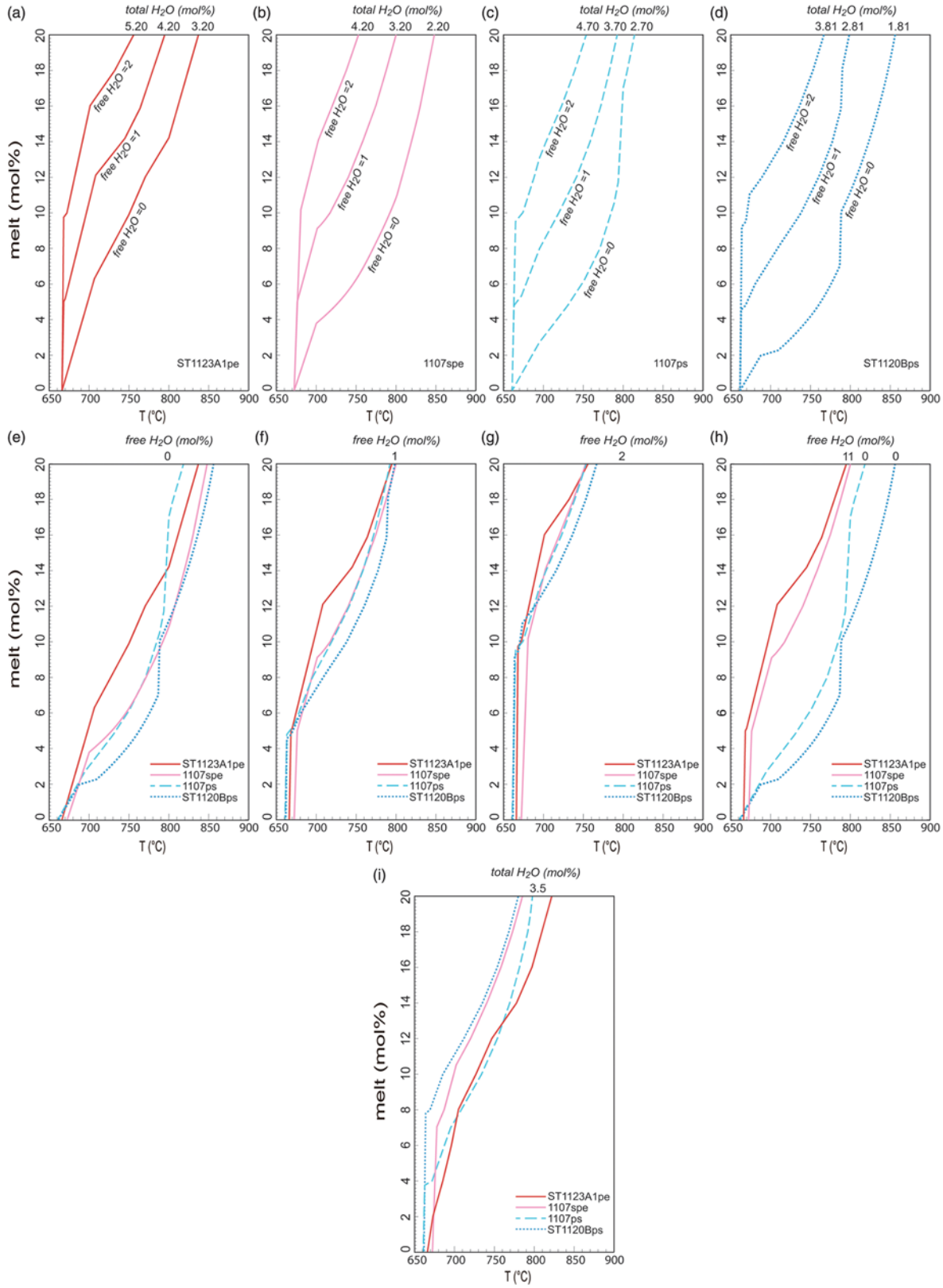

Fig. 7. (Colour online) Melt production as a function of temperature and water amount calculated at 3 kbar on the basis of the pseudosections in Figure 5. (a) ST1123A1pe. (b) 1107spe. (c) High-ferromagnesian 1107ps. (d) ST1120Bps. The melt production of different samples is compiled at specific water conditions of (e) free $H_2O = 0$; (f) free $H_2O = 1$ mol. %; (g) free $H_2O = 2$ mol. %; and (h) free $H_2O = 1$ mol. % for pelitic samples and 2 mol. % for psammitic samples. (i) Total $H_2O = 3.5$ mol. % for all samples. The water content (total H_2O) needed to just saturate the pelitic, semi-pelitic and high- and low-ferromagnesian psammitic compositions at solidus conditions are ˜3.20, 2.20, 2.70 and 1.81 mol. %, respectively.

https://doi.org/10.1017/S001675681800078X Published online by Cambridge University Press

of biotite and development of orthopyroxene occurs (Fig. 7a–e). Pelitic to semi-pelitic migmatite can thus be predicted to be more fertile than psammitic migmatite for lower temperature granulite-facies conditions, the potential fertility relationships flipping at high-*T* granulite-facies conditions (see also White *et al.* 2003).

Minor free water facilitates the melting of the four types of rocks, and ~5 mol.% melt is expected at just above the solidus for all when there is 1 mol.% free water (Fig. 7a–d, f). In this situation, all rocks have a steep initial slope of *T* versus melt fraction and obtain a melt volume of 7 mol.% between 680 and 700 °C (Fig. 7f). For the pelitic composition ST1123A, melt amounts to ~12 mol.% before all biotite is consumed at just above 700 °C, whereas the semi-pelitic and psammitic compositions produce less melt (8–9 mol.%). Between 700 and 800 °C, the pelitic composition is more fertile than the semi-pelitic and psammitic compositions, but the discrepancy in melt production shrinks in comparison with that modelled with low water content (free $H_2O = 0$). After biotite is consumed at ~790 °C, psammitic compositions obtain a high melt production comparable with that for pelitic compositions (Fig. 7f). If the free water at the solidus is as high as 2 mol.%, both pelitic and psammitic rocks will produce very high volumes of melt of ~10 mol.% at just above the solidus. The pelitic composition is more fertile than the semi-pelitic and psammitic compositions before it is surpassed by the semi-pelitic (1107spe) and psammitic (1107ps) compositions at 750 °C. At moderate temperatures, the four compositions show no significant difference in melt production, with a highest discrepancy of ~3 mol.%. In general, the addition of minor free water increases the melt fraction significantly: for example, at 750 °C the addition of 2 mol.% H_2O almost doubles the melt fraction for the pelitic composition (Fig. 7a) and nearly trebles it for the semi-pelitic and psammitic compositions (Fig. 7b–d).

The melt and residuum compositions for the representative pelitic, semi-pelitic and high- and low-ferromagnesian psammitic rocks at Mt Stafford were calculated from 700 °C to 850 °C at 3 kbar. The effect of varying conditions of free water (0, 1 and 2 mol.%) at the solidus were evaluated. Melt compositions are listed in Table 2 and shown in Figure 8, whereas the residuum compositions were compiled and illustrated in Table 3 and Figure 9. All melt and residuum calculations were performed in closed-system conditions.

6.c. *P–T* diagrams

As illustrated by the *T–X(H$_2$O)* pseudosections (Fig. 5a–d), the water content (total H_2O) needed to just saturate the pelitic, semi-pelitic and high- and low-ferromagnesian psammitic compositions at solidus conditions are ~3.20, 2.20, 2.70 and 1.81 mol.%, respectively. At such conditions, there is virtually no free water (free $H_2O = 0$) in the rocks at the solidus for $P \approx 3$ kbar. *P–T* pseudosections were constructed for the pelitic, semi-pelitic and psammitic compositions at the condition free $H_2O = 0$ for a *P–T* range of 2.5–4.5 kbar, at 650–900 °C (Fig. 10a–h). As the water-bearing minerals (muscovite) dehydrate just before the solidus, it is likely that the metasedimentary rocks have variable amounts of free water when they just reach their solidus. The situation that each rock system has 1 mol.% free water at the solidus was also considered, and the *P–T* pseudosections were calculated with total water contents of ~4.20, 3.20, 3.70 and 2.81 mol.% for the pelitic, semi-pelitic and high- and low- ferromagnesian psammitic compositions, respectively (Fig. 11a–h). The bulk compositions used for the calculations are listed in Table 1.

In general, the topologies of the phase relationships for pelitic, semi-pelitic and high- and low-ferromagnesian psammitic compositions with higher water contents (free $H_2O = 1$ mol.%) are similar to those with lower water contents (free $H_2O = 0$), particularly for the psammitic samples (1107ps and ST1120B). However, the increase in free water in the pelitic sample ST1123A1 shrinks the stability field of quartz and sillimanite to a lower temperature and expands the low-*T* limit of spinel. The high-*T* limit of plagioclase for semi-pelitic sample 1107spe was also shifted to a lower temperature by the increase in free water.

6.d. Melt development along the regional metamorphic field gradient

As the progress of melting was principally controlled by temperature, the modelled fixed pressure of 3 kbar reflects well the changes observed along the regional metamorphic field gradient. A minor variation in pressure will not significantly affect melt productivity (Figs 10, 11). Where there is virtually no free water at the solidus, pelitic sample ST1123A1 is predicted to have ~8 mol.% melt at 750 °C and 3.6 kbar (largely corresponds to Zone 3; White *et al.* 2003), and ~14 mol.% at 800 °C and 3.75 kbar (Zone 4). The ingress of minor free water (1 mol.%) will result in an additional ~6 mol.% melt along the gradient (Figs 10, 11). Both semi-pelitic sample 1107spe and high-ferromagnesian psammitic sample 1107ps are predicted to have ~5 mol.% melt at 750 °C and 3.6 kbar (Zone 3) but produce ~9 mol.% and ~13 mol.% melt, respectively, at 800 °C and 3.75 kbar (Zone 4) when water contents are low. The ingress of 1 mol.% free water to the samples is predicted to be accompanied by an increase of 6–7 mol.% melt at the prevailing conditions. Where there is no free water at solidus in the psammitic sample ST1120B, only ~3 mol.% melt could be expected at Zone 3 conditions, in contrast to ~10 mol.% at Zone 4. With slightly more water (free $H_2O = 1$ mol.%), the melt production of ST1120B is predicted to increase by ~7 mol.%.

The melt and residuum compositions were calculated for each of the bulk compositions at *P–T* conditions of 750 °C at 3.60 kbar and 800 °C at 3.75 kbar along the model local gradient, generally corresponding to the Zone 3 and Zone 4 conditions where melt loss could be expected to have occurred (White *et al.* 2003). The calculated melt and residuum compositions are listed in online Supplementary Material Tables S2 and S3. All melt was assumed to have been lost from the system at these conditions; therefore, the residual compositions reflect extreme values. The calculated compositions are basically similar to those calculated at the fixed pressure of 3 kbar. The slight variation in pressure does not change the model melt and residuum compositions markedly.

7. Discussion

As rocks in the lower to mid-crust contain small volumes of free water because of low porosity, fluid-absent melting is considered to be the dominant partial melting process (e.g. Thompson, 1982; Powell, 1983; Clemens & Vielzeuf, 1987). However, the ingress of H_2O into high-grade metamorphic rocks can promote additional melting (e.g. Brown, 2010, Yakymchuk & Brown, 2014) in circumstances involving shear zones (Johnson *et al.* 2001; Slagstad *et al.* 2005; Berger *et al.* 2008; Genier *et al.* 2008; Sawyer, 2010; Reichardt & Weinberg, 2012; Carvalho *et al.* 2016), extensional fracture systems (e.g. Ward *et al.* 2008) and contact aureoles (Pattison & Harte, 1988; Johnson *et al.* 2003, 2011; Droop & Brodie, 2012). Melting rocks may also obtain additional water from those adjacent rocks that have solidi of higher temperature and

https://doi.org/10.1017/S001675681800078X Published online by Cambridge University Press

Table 2. The model melt compositions at 3 kbar for the metasedimentary compositions of varying water activities (wt %)

ST1123A1pe	SiO_2	Al_2O_3	CaO	MgO	FeO	Na_2O	K_2O	MgO + FeO
Total H_2O = 3.2 mol. % (free H_2O = 0)								
700 °C	77.90	12.92	0.28	0.01	0.11	2.73	6.04	0.12
750 °C	77.22	13.40	0.38	0.02	0.19	2.37	6.41	0.21
800 °C	74.55	15.17	0.50	0.03	0.35	2.44	6.96	0.38
850 °C	72.67	16.55	0.65	0.04	0.46	2.27	7.37	0.50
Total H_2O = 4.2 mol. % (free H_2O = 1 mol %)								
700 °C	77.95	12.89	0.29	0.01	0.11	2.66	6.10	0.12
750 °C	75.29	14.57	0.41	0.02	0.24	2.69	6.78	0.26
800 °C	73.42	15.86	0.53	0.03	0.35	2.55	7.25	0.39
850 °C	71.94	16.83	0.68	0.06	0.52	2.30	7.67	0.58
Total H_2O = 5.2 mol. % (free H_2O = 2 mol.%)								
700 °C	78.00	12.84	0.30	0.01	0.11	2.59	6.15	0.12
750 °C	74.08	15.29	0.43	0.02	0.26	2.84	7.07	0.29
800 °C	72.71	16.30	0.56	0.03	0.34	2.55	7.49	0.38
850 °C	71.42	16.88	0.72	0.08	0.65	2.29	7.96	0.73
1107spe	**SiO_2**	**Al_2O_3**	**CaO**	**MgO**	**FeO**	**Na_2O**	**K_2O**	**MgO + FeO**
Total H_2O = 2.2 mol. % (free H_2O = 0)								
700 °C	78.34	12.58	0.36	0.01	0.09	2.12	6.49	0.10
750 °C	77.60	13.13	0.46	0.01	0.13	1.83	6.83	0.15
800 °C	76.79	13.77	0.58	0.02	0.19	1.56	7.10	0.21
850 °C	76.03	14.39	0.61	0.03	0.27	1.31	7.35	0.30
Total H_2O = 3.2 mol. % (free H_2O = 1 mol. %)								
700 °C	78.44	12.51	0.38	0.01	0.09	1.99	6.59	0.10
750 °C	77.69	13.06	0.48	0.01	0.13	1.68	6.94	0.15
800 °C	76.86	13.70	0.61	0.02	0.19	1.42	7.20	0.21
850 °C	76.29	14.19	0.48	0.03	0.27	1.18	7.56	0.29
Total H_2O = 4.2 mol. % (free H_2O = 2 mol. %)								
700 °C	78.55	12.42	0.39	0.01	0.08	1.85	6.69	0.09
750 °C	77.78	12.98	0.51	0.01	0.13	1.54	7.04	0.14
800 °C	77.07	13.54	0.53	0.02	0.19	1.30	7.36	0.21
850 °C	76.51	14.02	0.39	0.03	0.26	1.06	7.73	0.29
1107ps	**SiO_2**	**Al_2O_3**	**CaO**	**MgO**	**FeO**	**Na_2O**	**K_2O**	**MgO + FeO**
Total H_2O = 2.7 mol. % (free H_2O = 0)								
700 °C	77.84	12.95	0.26	0.01	0.11	2.89	5.93	0.13
750 °C	77.32	12.81	0.36	0.06	0.55	2.54	6.36	0.61
800 °C	76.26	12.35	0.53	0.21	1.93	1.86	6.87	2.14
850 °C	75.48	12.33	0.45	0.30	2.66	1.58	7.20	2.96
Total H_2O = 3.7 mol. % (free H_2O = 1 mol. %)								
700 °C	77.95	12.87	0.28	0.01	0.11	2.73	6.05	0.12
750 °C	77.46	12.73	0.39	0.05	0.52	2.36	6.50	0.57
800 °C	76.38	12.25	0.49	0.21	1.93	1.77	6.98	2.14
850 °C	75.78	12.13	0.36	0.30	2.59	1.41	7.42	2.89
Total H_2O = 4.7 mol. % (free H_2O = 2 mol. %)								
700 °C	78.06	12.78	0.30	0.01	0.10	2.55	6.18	0.11
750 °C	77.59	12.64	0.42	0.05	0.48	2.17	6.64	0.54
800 °C	76.47	12.18	0.45	0.20	1.94	1.72	7.05	2.15
850 °C	76.05	11.95	0.30	0.30	2.52	1.26	7.62	2.82

(*Continued*)

https://doi.org/10.1017/S001675681800078X Published online by Cambridge University Press

Table 2. (*Continued*)

ST1120Bps	SiO_2	Al_2O_3	CaO	MgO	FeO	Na_2O	K_2O	MgO + FeO
Total H_2O = 1.81 mol. % (free H_2O = 0)								
700 °C	77.65	13.08	0.21	0.01	0.12	3.27	5.66	0.14
750 °C	77.00	13.01	0.28	0.07	0.62	3.11	5.92	0.69
800 °C	75.80	12.75	0.38	0.22	1.94	2.74	6.17	2.16
850 °C	74.81	12.91	0.48	0.31	2.68	2.50	6.31	3.00
Total H_2O = 2.81 mol. % (free H_2O = 1 mol. %)								
700 °C	77.69	13.05	0.22	0.01	0.12	3.20	5.71	0.13
750 °C	77.05	12.98	0.29	0.07	0.60	3.02	5.99	0.67
800 °C	75.89	12.70	0.40	0.22	1.90	2.64	6.26	2.12
850 °C	74.96	12.86	0.50	0.32	2.56	2.39	6.42	2.87
Total H_2O = 3.81 mol. % (free H_2O = 2 mol. %)								
700 °C	77.74	13.01	0.23	0.01	0.12	3.12	5.77	0.13
750 °C	77.13	12.94	0.30	0.06	0.58	2.93	6.06	0.64
800 °C	75.98	12.64	0.42	0.22	1.85	2.53	6.36	2.08
850 °C	75.11	12.81	0.52	0.32	2.43	2.27	6.54	2.75

are undergoing sub-solidus dehydration (e.g. White *et al.* 2005). Even for circumstances involving very small quantities, such water ingress can dramatically influence a variety of physical and chemical properties of geological materials such as melting temperatures, melt production, melt chemistry, viscosity and density, phase equilibria and reaction kinetics (e.g. Weinberg & Hasalová, 2015). For high-temperature contact metamorphic aureoles, heating to peak temperatures above the solidus can be very rapid, and water ingress could potentially be derived from the preservation of H_2O liberated by hydrous mineral breakdown at sub-solidus (e.g. Droop & Brodie, 2012), the retention of H_2O in metastable hydrate minerals to super-solidus conditions (e.g. Buick *et al.* 2004; Johnson *et al.* 2011), the addition of H_2O from interlayered rocks (e.g. Rigby *et al.* 2008) and the transient access to external H_2O, such as derived from crystallization of the nearby pluton or from further away. With the possible ingress of water being considered, below we discuss the possible melt evolution and the effect of melt loss for the metasedimentary rocks in the regional contact aureole at Mt Stafford.

7.a. Melt fertility and the effect of minor free water

Metasedimentary rocks similar to those at Mt Stafford have the potential to produce large partial melt fractions, depending on details of the *P–T* conditions and compositions involved (Le Breton & Thompson, 1988; Puziewicz & Johannes, 1988; Vielzeuf & Holloway, 1988; Holtz & Johannes, 1991; Patiño-Douce & Johnson, 1991; Skjerlie & Johnston, 1992; Vielzeuf & Montel, 1994; Stevens *et al.* 1997). The modelling in this study shows that with low water contents (free $H_2O = 0$) there are remarkable differences in the temperature conditions of key melting steps for the pelitic, semi-pelitic and high- and low-ferromagnesian psammitic compositions at Mt Stafford (Fig. 7a–e). In particular, there is a wide range of modelled melt modes, controlled by composition, between 700 and 800 °C. In this temperature range, the pelitic composition (ST1123A1) is predicted to have the highest proportion of melt, and the ferromagnesian-poor psammitic composition (ST1120Bps) predicted to have the lowest proportion, with the largest difference between them being ~6 mol.% (Fig. 7e). Metapsammite of higher ferromagnesian content (1107ps) is predicted to have ~2 mol.% more melt than metapsammite of lower ferromagnesian content (ST1120Bps) for the temperature range of common granulite-facies rocks (700–800 °C), and to have higher melt proportions than the modelled semi-pelite (1107spe) at $T > 780$ °C. These relationships indicate a dependence of melt productivity on whole-rock ferromagnesian content, in assemblages principally controlled by biotite mode (White *et al.* 2003). At water-undersaturated conditions, the whole-rock composition is the overriding factor controlling melt production (Patiño-Douce & Johnson, 1991), but a minor increase in free water can significantly boost melt production (Fig. 7f, g). A small discrepancy in the volume of free water between otherwise similar layers thus has the potential to significantly expand the range of melt production (Fig. 7h). Along the given field array, the modelling shows the pelitic rocks at Mt Stafford develop much more melt than psammitic compositions, with a larger difference than that modelled with low water content (~6 mol.% melt when free $H_2O = 0$; Fig. 7e). This distinction has been attributed to the effect of minor elements such as boron, with tourmaline being more abundant in pelitic rocks (Greenfield *et al.* 1996, 1998; White *et al.* 2003). A higher boron content is predicted to displace the temperature of the solidi for the natural Mt Stafford pelitic rock to lower temperature conditions (Chorlton & Martin, 1978; Pichavant, 1981; Bénard *et al.* 1985). However, experiments conducted by EM Spicer (unpub. Ph.D. thesis, Univ. Stellenbosch, 2011) on boron-bearing samples from Mt Stafford would appear to indicate that the presence of tourmaline does not markedly affect fluid-absent incongruent melting reactions. Though the possible impact of some other minor elements cannot be ruled out, variations in retained free water in the rocks undergoing partial melting may play an influential role in expanding the difference in melt production between pelitic and psammitic rocks.

If an interconnected network of grain edge melt channels is developed, melt loss can be expected to occur, especially when the rocks are compacted and/or deformed (e.g. McKenzie, 1984;

https://doi.org/10.1017/S001675681800078X Published online by Cambridge University Press

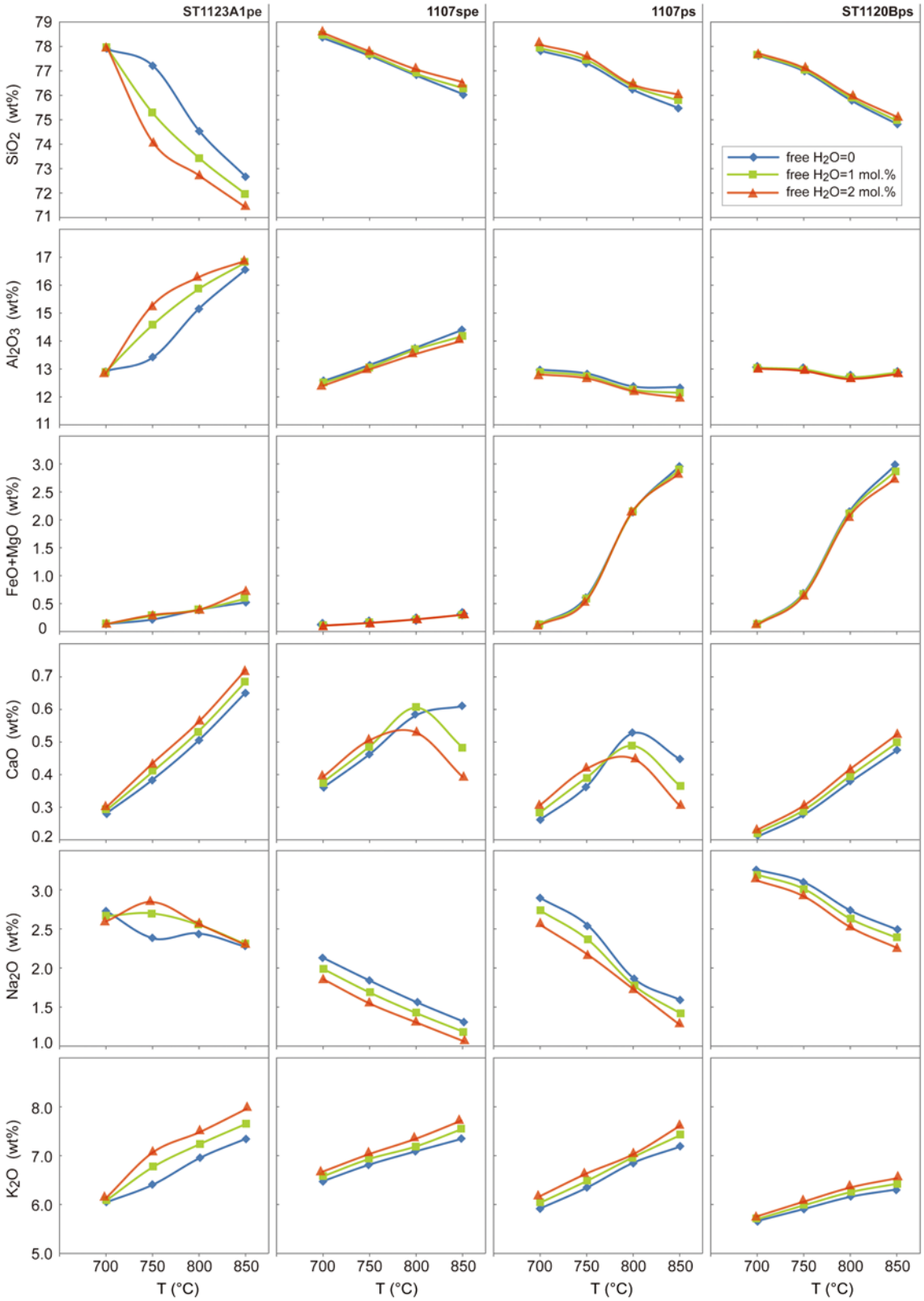

Fig. 8. (Colour online) Melt compositions as a function of temperature and water amount calculated at 3 kbar for the metasedimentary rocks.

Rosenberg & Handy, 2005). Experiments and numerical modelling suggest low thresholds for melt extraction (Laporte *et al.* 1997; Rabinowicz & Vigneresse, 2004). A maximum value for this critical threshold is suggested to be ~7 vol.%, based on an analysis of deformation experiments on melt-bearing aggregates, corresponding to the point at which more than 80% of grain boundaries become melt bearing (referred to as the melt connectivity transition (MCT); Rosenberg & Handy, 2005; Yakymchuk & Brown,

https://doi.org/10.1017/S001675681800078X Published online by Cambridge University Press

Table 3. The model residuum compositions at 3 kbar for the metasedimentary compositions of varying water activities. The melt mode removed from the system is also shown

ST1123A1pe	SiO_2 (wt %)	Al_2O_3 (wt %)	CaO (wt %)	MgO (wt %)	Fe_2O_3 (wt %)	K_2O (wt %)	Na_2O (wt %)	TiO_2 (wt %)	Fe_2O_3 + MgO (wt %)	CaO + K_2O + Na_2O (wt %)	Melt removed (mol. %)
Total H_2O = 3.2 mol. % (free H_2O = 0)											
700 °C	56.93	24.04	0.46	2.00	7.26	7.22	1.26	0.82	9.26	8.94	5.25
750 °C	55.99	24.49	0.46	2.13	7.59	7.25	1.22	0.86	9.72	8.93	10.34
800 °C	55.51	24.64	0.45	2.22	7.89	7.22	1.16	0.90	10.11	8.83	14.40
850 °C	54.07	25.15	0.41	2.47	8.67	7.18	1.08	0.97	11.13	8.67	23.55
Total H_2O = 4.2 mol. % (free H_2O = 1 mol. %)											
700 °C	56.00	24.53	0.47	2.08	7.59	7.27	1.20	0.86	9.68	8.94	10.46
750 °C	55.46	24.72	0.46	2.22	7.87	7.24	1.13	0.90	10.09	8.83	14.61
800 °C	54.52	25.08	0.44	2.38	8.39	7.19	1.06	0.95	10.76	8.69	20.87
850 °C	52.58	25.81	0.37	2.71	9.45	7.07	0.95	1.06	12.16	8.39	31.48
Total H_2O = 5.2 mol. % (free H_2O = 2 mol. %)											
700 °C	54.95	25.07	0.48	2.18	7.96	7.33	1.14	0.90	10.14	8.94	15.67
750 °C	54.82	25.02	0.46	2.32	8.20	7.21	1.04	0.93	10.52	8.71	19.25
800 °C	53.44	25.54	0.43	2.55	8.96	7.13	0.95	1.00	11.51	8.51	27.17
850 °C	50.98	26.62	0.32	2.97	10.25	6.87	0.83	1.15	13.22	8.02	38.57
1107spe	SiO_2 (wt %)	Al_2O_3 (wt %)	CaO (wt %)	MgO (wt %)	Fe_2O_3 (wt %)	K_2O (wt %)	Na_2O (wt %)	TiO_2 (wt %)	Fe_2O_3 + MgO (wt %)	CaO + K_2O + Na_2O (wt %)	Melt removed (mol. %)
Total H_2O = 2.2 mol. % (free H_2O = 0)											
700 °C	68.93	17.47	0.17	1.75	6.02	4.48	0.48	0.70	7.77	5.13	3.53
750 °C	68.75	17.54	0.16	1.80	6.17	4.41	0.45	0.72	7.98	5.02	6.28
800 °C	68.44	17.62	0.13	1.89	6.47	4.27	0.42	0.75	8.37	4.82	11.10
850 °C	67.85	17.71	0.08	2.10	7.15	3.92	0.35	0.84	9.26	4.35	20.29
Total H_2O = 3.2 mol. % (free H_2O = 1 mol. %)											
700 °C	68.53	17.66	0.16	1.83	6.29	4.38	0.42	0.73	8.12	4.96	8.62
750 °C	68.20	17.78	0.14	1.92	6.57	4.24	0.38	0.76	8.49	4.77	12.96
800 °C	67.67	17.91	0.09	2.08	7.11	3.97	0.33	0.83	9.19	4.39	20.11
850 °C	66.52	18.13	0.05	2.46	8.34	3.28	0.25	0.98	10.81	3.57	32.70
Total H_2O = 4.2 mol. % (free H_2O = 2 mol. %)											
700 °C	68.07	17.89	0.15	1.91	6.59	4.27	0.36	0.76	8.50	4.78	13.70
750 °C	67.55	18.07	0.11	2.06	7.03	4.04	0.32	0.82	9.09	4.47	19.63
800 °C	66.68	18.31	0.06	2.31	7.88	3.58	0.26	0.92	10.19	3.89	28.85
850 °C	64.56	18.77	0.02	2.97	10.04	2.30	0.15	1.19	13.01	2.47	44.89
1107ps	SiO_2 (wt %)	Al_2O_3 (wt %)	CaO (wt %)	MgO (wt %)	Fe_2O_3 (wt %)	K_2O (wt %)	Na_2O (wt %)	TiO_2 (wt %)	Fe_2O_3 + MgO (wt %)	CaO + K_2O + Na_2O (wt %)	Melt removed (mol. %)
Total H_2O = 2.7 mol. % (free H_2O = 0)											
700 °C	72.83	12.79	0.15	1.61	7.59	3.86	0.57	0.61	9.20	4.58	3.23
750 °C	72.72	12.79	0.14	1.66	7.78	3.78	0.52	0.62	9.44	4.44	6.26
800 °C	72.35	12.83	0.08	1.92	8.35	3.36	0.40	0.71	10.26	3.84	17.54
850 °C	72.20	12.82	0.05	2.13	8.94	2.76	0.30	0.81	11.06	3.11	27.78
Total H_2O = 3.7 mol. % (free H_2O = 1 mol. %)											
700 °C	72.61	12.76	0.14	1.68	7.95	3.76	0.48	0.63	9.63	4.37	8.45
750 °C	72.43	12.76	0.12	1.76	8.26	3.59	0.42	0.66	10.02	4.13	12.85

(*Continued*)

https://doi.org/10.1017/S001675681800078X Published online by Cambridge University Press

Table 3. (*Continued*)

1107ps	SiO_2 (wt %)	Al_2O_3 (wt %)	CaO (wt %)	MgO (wt %)	Fe_2O_3 (wt %)	K_2O (wt %)	Na_2O (wt %)	TiO_2 (wt %)	Fe_2O_3 + MgO (wt %)	CaO + K_2O + Na_2O (wt %)	Melt removed (mol. %)
800 °C	72.04	12.87	0.05	2.04	8.90	3.03	0.30	0.77	10.93	3.39	24.62
850 °C	71.50	12.95	0.02	2.47	10.12	1.80	0.16	0.96	12.60	1.99	39.73
Total H_2O = 4.7 mol. % (free H_2O = 2 mol. %)											
700 °C	72.36	12.73	0.13	1.76	8.34	3.63	0.39	0.67	10.11	4.14	13.65
750 °C	72.08	12.74	0.10	1.88	8.83	3.36	0.32	0.70	10.71	3.77	19.42
800 °C	71.73	12.91	0.03	2.14	9.45	2.70	0.21	0.82	11.60	2.94	30.53
850 °C	70.37	13.21	0.00	2.98	11.90	0.32	0.02	1.19	14.88	0.35	51.47
ST1120Bps	SiO_2 (wt %)	Al_2O_3 (wt %)	CaO (wt %)	MgO (wt %)	Fe_2O_3 (wt %)	K_2O (wt %)	Na_2O (wt %)	TiO_2 (wt %)	Fe_2O_3 + MgO (wt %)	CaO + K_2O + Na_2O (wt %)	Melt removed (mol. %)
Total H_2O = 1.81 mol. % (free H_2O = 0)											
700 °C	76.68	12.08	0.53	1.20	4.32	3.46	1.21	0.53	5.52	5.20	2.35
750 °C	76.69	12.05	0.53	1.22	4.39	3.41	1.18	0.53	5.61	5.12	4.39
800 °C	76.81	11.99	0.54	1.34	4.48	3.20	1.08	0.57	5.81	4.82	11.46
850 °C	77.19	11.84	0.54	1.42	4.51	2.91	0.98	0.62	5.93	4.43	18.72
Total H_2O = 2.81 mol. % (free H_2O = 1 mol. %)											
700 °C	76.66	12.00	0.55	1.25	4.52	3.36	1.12	0.55	5.77	5.02	7.58
750 °C	76.69	11.96	0.55	1.30	4.63	3.24	1.06	0.56	5.93	4.85	11.04
800 °C	76.94	11.89	0.55	1.45	4.73	2.88	0.93	0.63	6.18	4.37	20.36
850 °C	77.65	11.58	0.54	1.61	4.85	2.27	0.77	0.73	6.46	3.58	31.44
Total H_2O = 3.81 mol. % (free H_2O = 2 mol. %)											
700 °C	76.62	11.92	0.56	1.31	4.74	3.24	1.02	0.58	6.05	4.82	12.82
750 °C	76.69	11.87	0.57	1.38	4.92	3.04	0.94	0.60	6.30	4.54	17.67
800 °C	77.09	11.77	0.57	1.59	5.05	2.46	0.78	0.70	6.65	3.80	29.24
850 °C	78.25	11.24	0.53	1.90	5.40	1.28	0.50	0.89	7.30	2.32	44.08

2014). Rocks with higher melt proportions may lose melt easily, especially when there is deformation. Obvious centimetre- to decimetre-scale veins may develop at the solid-to-liquid transition (SLT; Rosenberg & Handy, 2005).

Modelling shows that with low water content (free $H_2O = 0$), the melt mode of pelitic sample ST1123A1 will reach 7 mol.% (~7 vol.%; also Yakymchuk & Brown, 2014) at ~715 °C, followed by semi-pelitic sample 1107spe and high-ferromagnesian psammitic sample 1107ps at ~750 °C (Fig. 7e). The psammitic sample ST1102B does not produce as much melt as 7 mol.% until ~790 °C when orthopyroxene appears and biotite disappears (Fig. 7e). Addition of minor free water can remarkably facilitate melting just above the solidus. When there is ~1 mol.% free water at the solidus, all of the rocks will produce as much as 7 mol.% melt from 680 °C to 700 °C (Fig. 7f). The increase in free water to 2 mol.% will decrease the temperature for 7 mol.% melt production by ~20 °C (Fig. 7g). Minor additional free water will result in significant melting and likely melt loss at high-grade zones.

Along the Mt Stafford metamorphic field gradient, pelitic rocks were observed to have produced remarkably more melt than interlayered psammitic rocks in the field, with leucosome proportions of up to 20% or more in zones 3 and 4, forming extensive vein networks and locally diatexite (Vernon *et al.* 1990; Greenfield *et al.* 1996, 1998). With low water content (free $H_2O = 0$), the pelitic sample (ST1123A1) could produce melt of ~10 mol.% at Zone 3 conditions (750 °C) and no more than ~15 mol.% at Zone 4 conditions (800 °C), lower than the melt volume estimated from corresponding fertile pelitic layers in the field (Fig. 7a–e). A slight increase in free water (e.g. 1 mol.%) can raise the melt production of the pelitic rocks to the level of the field observation (Fig. 7a–f). However, the modelling shows that if there is any, the amount of additional H_2O must be limited both at low- and high-grade zones, for example no more than 2 mol.%, otherwise voluminous melt will develop through the field thermal gradient, which is inconsistent with the delicate mineral textures observed in zones 1 and 2 and the melt modes estimated at zones 3 and 4 (Fig. 7a–g). As both the interlayered pelitic and psammitic rocks crossed solidi at the lower temperature side of the aureole, the psammitic layers in the high-grade zones 3 and 4 cannot be the source of free water for the neighbouring pelitic layers, as any H_2O from the psammitic layers will enter local melt. Where psammitic rocks have total water contents comparable to that of adjacent pelitic rocks, for example in the situation of an external influx (e.g. Craven *et al.* 2013), they will not be much less fertile than the pelitic rocks (Fig. 7i). The difference in melt produced between pelitic and psammitic layers rules out the possibility of any significant influx of externally derived H_2O into the psammitic layers. The melting processes of rocks within a high-temperature contact aureole may

https://doi.org/10.1017/S001675681800078X Published online by Cambridge University Press

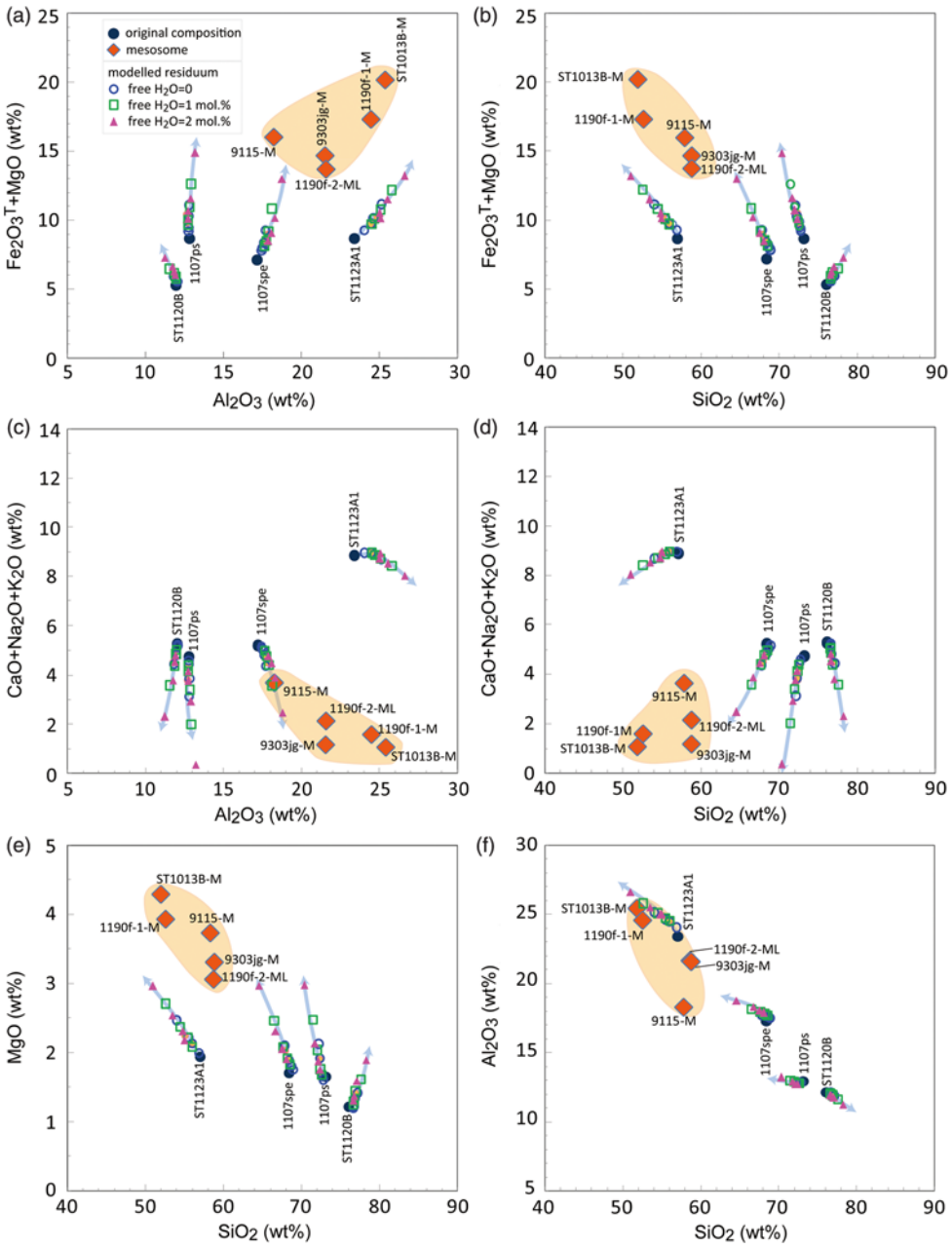

Fig. 9. (Colour online) Residuum compositions as a function of temperature and water amount calculated at 3 kbar for the metasedimentary rocks. The arrows show the direction of temperature increase in steps of 50 °C as in Table 3. The residuum becomes poorer in alkali composition and richer in ferromagnesian composition as temperature increases.

differ remarkably with distance from the heat source (e.g. Kerrick, 1991; Buick *et al.* 2004). At the higher-grade zones of a contact aureole, rapid heating could also cause reaction overstepping and metastable persistence of hydrous minerals (e.g. muscovite) to above the solidus, and consequently raise the water contents and corresponding melt mode in the system (Buick *et al.* 2004; Johnson *et al.* 2011). These mechanisms may have operated to some extent in the contact aureole at Mt Stafford, particularly for the high-grade zones close to the heat source, where rapid heating could more likely occur. The possible retention of higher water in pelite than in psammite above solidus is also consistent with the estimates of higher bound and pore water in pelite than psammite (e.g. Yardley, 2009).

Though the modelled melt production is evidently affected by variations in free water, mineral assemblages are not always sensitive to water activity at the *P–T* conditions similar to those at Mt Stafford (Figs 5, 10, 11). For pelitic ST1123A1 and semi-pelitic 1107spe compositions, the mineral stability boundaries below 710 °C are largely parallel to the $X(H_2O)$ axis for total H_2O ranging from 2 to 8 mol.% (Fig. 5a, b). Above 710 °C, the predicted mineral equilibria are generally bound by lines with negative slopes from higher to lower temperatures. The topologies indicate that for large variations in initial water content, for example from 2 to 8 mol.%, there is relatively little difference in the mineral assemblages developed along heating paths (vertical lines) for systems with different initial water contents. Many mineral assemblages occur over a wide range of water contents, for instance the kfs+sill+crd+qtz+liq+mag+ilm in the quinivariant field of 1107spe can have water contents ranging from ~1 to ~14 mol.% (Fig. 5b). For the ferromagnesian-rich psammitic rocks 1107ps and ST1120B, the occurrence of orthopyroxene is always accompanied by the disappearance of biotite at around 800 °C, regardless of any appreciable variation in initial water content (Fig. 5c, d). Like the pelite and semi-pelite, the major mineral assemblages of

https://doi.org/10.1017/S001675681800078X Published online by Cambridge University Press

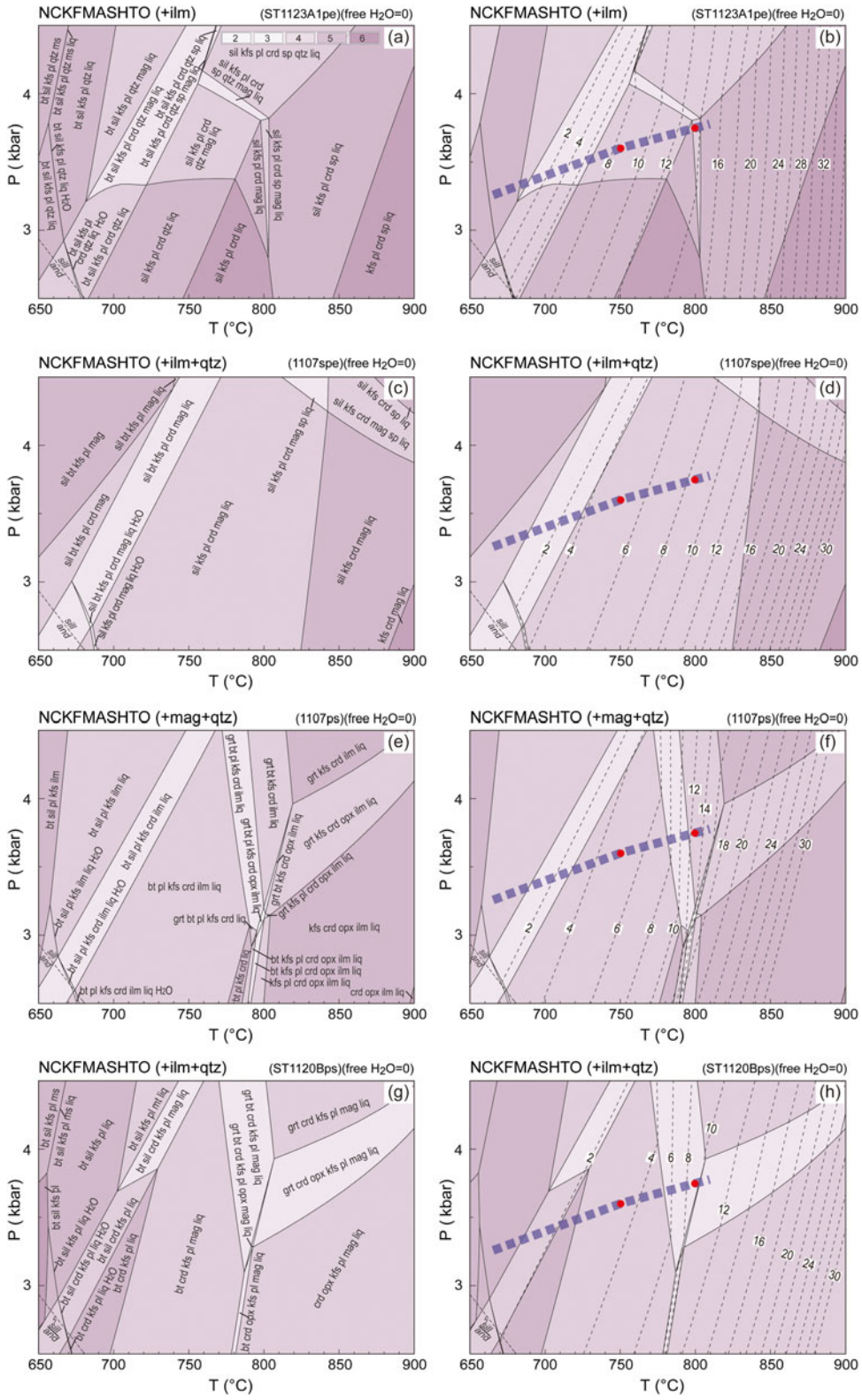

Fig. 10. (Colour online) *P–T* pseudosections for the representative metasedimentary samples with free $H_2O = 0$ at solidus. Calculated molar mode contours in per cent for melt are shown with dashed lines. Variance of equilibria in stability fields is indicated in the legend (a). (a, b) Pelitic sample ST1123A1. (c, d) Semi-pelitic sample 1107spe. (e, f) High-ferromagnesian psammitic sample 1107ps. (g, h) Psammitic sample ST1120Bps. The compositions used in calculations of the pseudosections are included in Table 1. The thick dashed lines on the figures represent a generalized field array (White *et al.* 2003). The red dots designate the *P–T* conditions for calculating melt and residuum compositions (online Supplementary Material Tables S2 and S3).

the psammitic rocks are not markedly affected by water activity. The main difference resultant upon increasing initial water will typically be the increased melt volume, rather than the nature of the paragenesis. Consequently, neither the melting reaction nor the mineral paragenesis alone is a reliable indicator of the volume of added H_2O.

7.b. Melt composition at low-pressure conditions

The composition of melt produced by fluid-absent or fluid-present partial melting in deep crustal settings can be examined by petrological melting experiments (Skjerlie *et al.* 1993; Patiño-Douce, 1996; Patiño-Douce & Harris, 1998; Koester *et al.* 2002) or forward modelling (e.g. Grant, 2009; White *et al.* 2011). There are

https://doi.org/10.1017/S001675681800078X Published online by Cambridge University Press

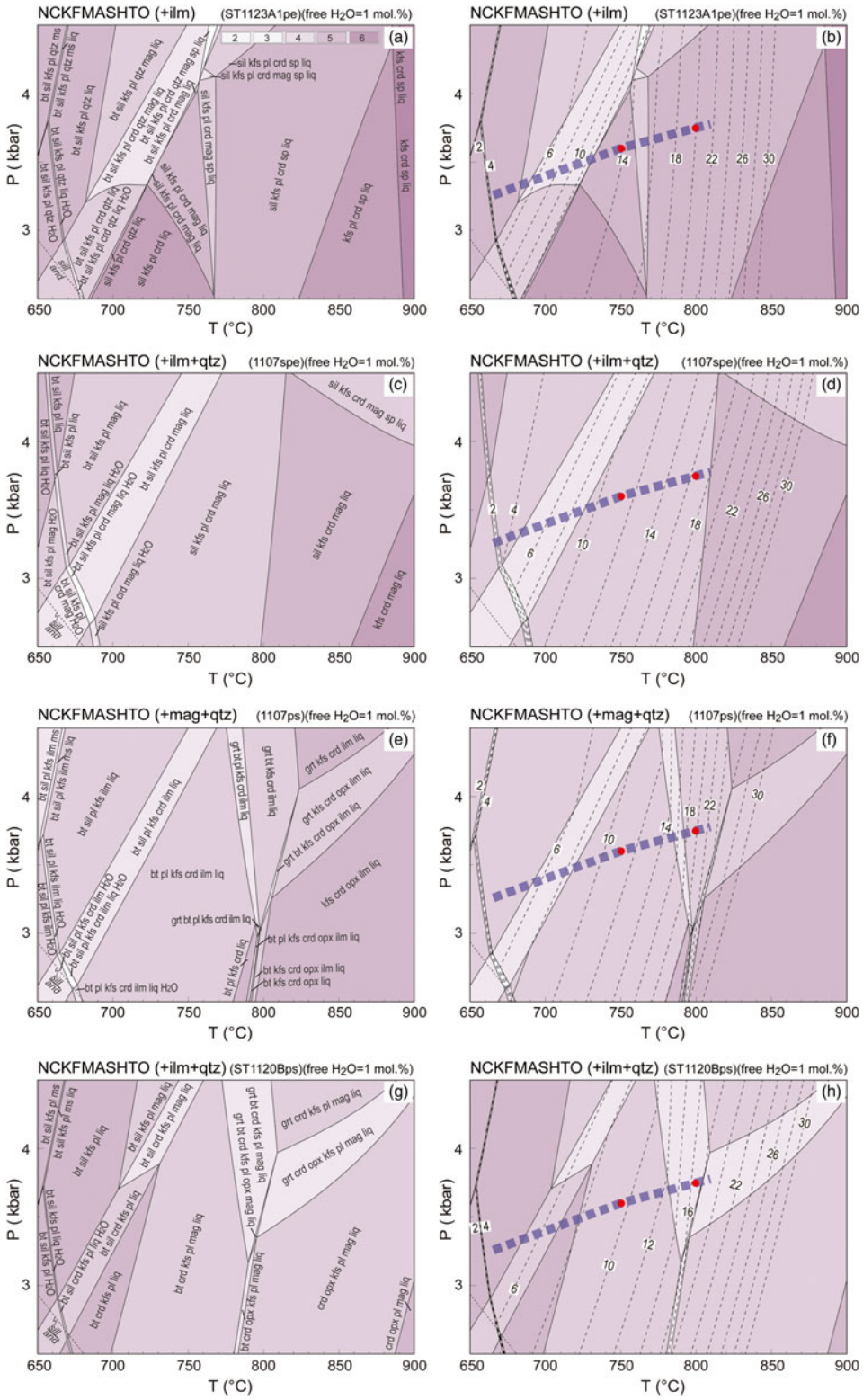

Fig. 11. (Colour online) *P–T* pseudosections for the representative metasedimentary samples with free $H_2O = 1$ at solidus. Calculated molar mode contours in per cent for melt are shown with dashed lines. Variance of equilibria in stability fields is indicated in the legend in (a). (a, b) Pelitic sample ST1123A1. (c, d) Semi-pelitic sample 1107spe. (e, f) High-ferromagnesian psammitic sample 1107ps. (g, h) Psammitic sample ST1120Bps. See Table 1 for the compositions used for the calculations. The thick dashed lines on the figures represent a generalized field array (also White *et al.* 2003). The red dots designate the *P–T* conditions for calculating melt and residuum compositions (online Supplementary Material Tables S2 and S3).

important consistencies in basic compositional trends and phase topologies between the modelling and experimental results, though there remain distinctions between the two approaches (White *et al.* 2011). Melt compositions derived from melt inclusions, experiments and thermodynamic modelling can be used as benchmarks to discuss the potential processes involved in the compositional evolution of leucosome and associated migmatite (e.g. Brown *et al.* 2016; Acosta-Vigil *et al.* 2017). Melt compositions calculated for the representative rock samples at Mt Stafford indicate strong dependencies on bulk composition and temperature rather than on water activity. With low water content (free $H_2O = 0$), the melts produced by the four metasedimentary samples are granitic (Fig. 12), being enriched in SiO_2, Al_2O_3 and K_2O contents (Table 2; Figs 7, 12, 13). Melt in pelitic sample ST1123A1 and semi-pelitic

https://doi.org/10.1017/S001675681800078X Published online by Cambridge University Press

sample 1107spe has a low ferromagnesian content that subtly increases from low to high temperatures, in contrast to a marked step in ferromagnesian content for psammitic samples ST1120B and 1107ps (Figs 7, 14). Compared with the results of relevant experiments conducted at higher pressures, the model melt compositions are enriched in K_2O and depleted in CaO (Fig. 12). The silica and soda contents of the melt decrease with temperature increases for all samples, whereas the ferromagnesian and potash contents increase. The calcium content increases with grade until plagioclase is consumed. For silica-rich rocks, the silica component in the melt does not decrease remarkably with increasing temperature, but for low-quartz pelitic samples (ST1123A1), the silica content of the melt drops markedly at high temperature (Table 2; Fig. 13). These variations demonstrate the dependence of the melt compositions on their bulk rock composition and reaction history.

The addition of free water changes the melt composition of the metasedimentary rocks in several ways. In general, any increase in water content will generate melt of higher potash content for all samples, but lower soda content for all but the pelitic sample ST1123A1. This result is different from the outcomes of higher pressure experiments conducted using pelitic muscovite schist (MS, Patiño-Douce & Harris, 1998) and metagreywacke (SBG, Patiño-Douce, 1996). In those experiments, the addition of water generated melt comparatively enriched in soda and depleted in potash at temperatures lower than the dehydration solidus (Patiño-Douce & McCarthy, 1998). The opposing trends can be attributed to differences in bulk composition and pressure at which the experiments were run, with and without free water. The ferromagnesian contents of the model melt are not obviously dependent on the volume of free water (Table 2; Fig. 8). Any addition of free water displaces the upper limit of plagioclase-bearing equilibria to a lower temperature, with the consequence that melt produced at a higher temperature than plagioclase stability has progressively less calcium. An increase in free water will result in a subtly higher calcium content when plagioclase is present, and the reverse when plagioclase has been consumed (Fig. 8). At water-rich conditions, the silica content of the melt modelled for pelitic sample ST1123A1 falls as grade increases, particularly at higher temperature conditions, in contrast to a subtle increase with grade for the semi-pelitic and psammitic samples (Fig. 8). The alumina content of the melt modelled at higher temperature conditions increased with the addition of free water for the pelitic sample ST1123A1, but subtly decreased for all other samples. However, in general, a minor increase in free water will have a relatively limited effect on the melt compositions modelled for the samples.

7.c. Effect of melt loss on residual composition

The greenschist- to granulite-facies transition at Mt Stafford is focused over a comparatively narrow ~5 km distance, and exposes an unusual series of migmatites which developed progressively greater proportions of melt at higher grades. High proportions of melt were most likely present in the highest-grade zones, with schlieren migmatite occurring as a transitional unit between bedded migmatite and metapelite-sourced diatexite (Greenfield *et al.* 1996). Modelling completed in this study predicts that the metasedimentary rocks at Mt Stafford would produce no less than 15% melt at ~800 °C at ~3 kbar (Zone 4). Migmatite with such high melt proportions will likely undergo melt loss and thus change the composition of the parent rock. To evaluate the effect of melt loss from the Mt Stafford metasedimentary rocks, residuum compositions were calculated considering different water contents (at 3 kbar) for the pelitic, semi-pelitic and high- and low-ferromagnesian psammitic samples (Table 3).

As mass balance is preserved at all scales during melting and melt segregation in the model system, a ternary K–(Na + Ca)–(Fe^* + Mg + Ti) plot (Fig. 14) can be used to track melt-residuum evolution (Solar & Brown, 2001). In such a model, the main residuum minerals involving cordierite, orthopyroxene, garnet and biotite lie close to the (Fe^* + Mg + Ti) apex or along the (Fe^* + Mg + Ti)–K edge of the ternary plot. The (Na + Ca)–K edge of the ternary diagram represents a plagioclase and K-feldspar join, along which melts produced from metasedimentary rocks can be expected to fall. With increasing temperature, the residuum compositions of the samples evolve progressively closer to the (Fe^* + Mg + Ti) apex. The trends are enhanced by the addition of minor free water. Residuum compositions have a strong dependence on the starting rock compositions. At the same *P*–*T* condition, rocks with high Fe^* –Mg–Ti ratios (e.g. 1107ps) are predicted to evolve residuum closer to the (Fe^* + Mg + Ti) apex. In the plot, the psammitic sample ST1120B and pelitic sample ST1123A1 have similar Fe^*–Mg–Ti ratios, but any addition of free water will shift the residuum of the sample ST1120B towards the (Fe^* + Mg + Ti) apex more dramatically than for sample ST1123A1. These trends reflect changes in the ratio of (Fe^* + Mg + Ti) to alkali content rather than the ferromagnesian content of the residuum. The residuum compositions predicted for sample ST1120B lie closer to the (Fe^* + Mg + Ti) apex than those of sample ST1123A1 and have lower ferromagnesian contents (Figs 9, 14). When contrasted with their starting bulk compositions, the ferromagnesian contents ($Fe_2O_3{}^T$ + MgO) of the model residuum increase with increasing temperature, whereas the total alkali contents (CaO + Na_2O + K_2O) decrease. Any added free water will exaggerate the enrichment of the ferromagnesian content and depletion of the alkali content. The alumina content of the pelitic and semi-pelitic residuum increases with temperature, but subtly decreases for the psammitic sample ST1120B (Fig. 9a, c, f). The potash contents of the residuum compositions of the pelitic sample (ST1123A1; with high initial potassium content) is predicted to increase subtly with melt loss, in contrast to the decrease in the potash contents of residua for semi-pelitic and psammitic compositions (Table 3).

A comparison between the modelled residuum compositions and the natural melanosome/mesosome illustrates that melt loss alone from the normal semi- or pelitic compositions as used for modelling cannot directly result in the extremely high ferromagnesian and low alkali compositions observed in the natural rocks. Even if free water content is increased to 2 mol.% – higher than could be expected for the field setting – the predicted residuum compositions do not explain the unusual ferromagnesian-rich, alkali-poor melanosome/mesosome samples (Table 3; Fig. 9). The unusual melanosome/mesosome samples may have originally had relatively high ferromagnesian and low alkali compositions in their protolith, or some other processes like chemical diffusion or metamorphic differentiation may play a role in changing the composition. In general, granulite-facies rocks are enriched in iron, magnesium and titanium and depleted in silica, soda and potash content (e.g. Redler *et al.* 2013). However, the origin of granulite with extremely high ferromagnesian and low alkali contents cannot always be completely attributed to melt loss. Primary composition has a basic control on the residual granulite composition. Systematic chemical analysis of the rocks from low (sub-solidus) to high grade (granulite facies) and modelling of compositional variation related to melt loss could

https://doi.org/10.1017/S001675681800078X Published online by Cambridge University Press

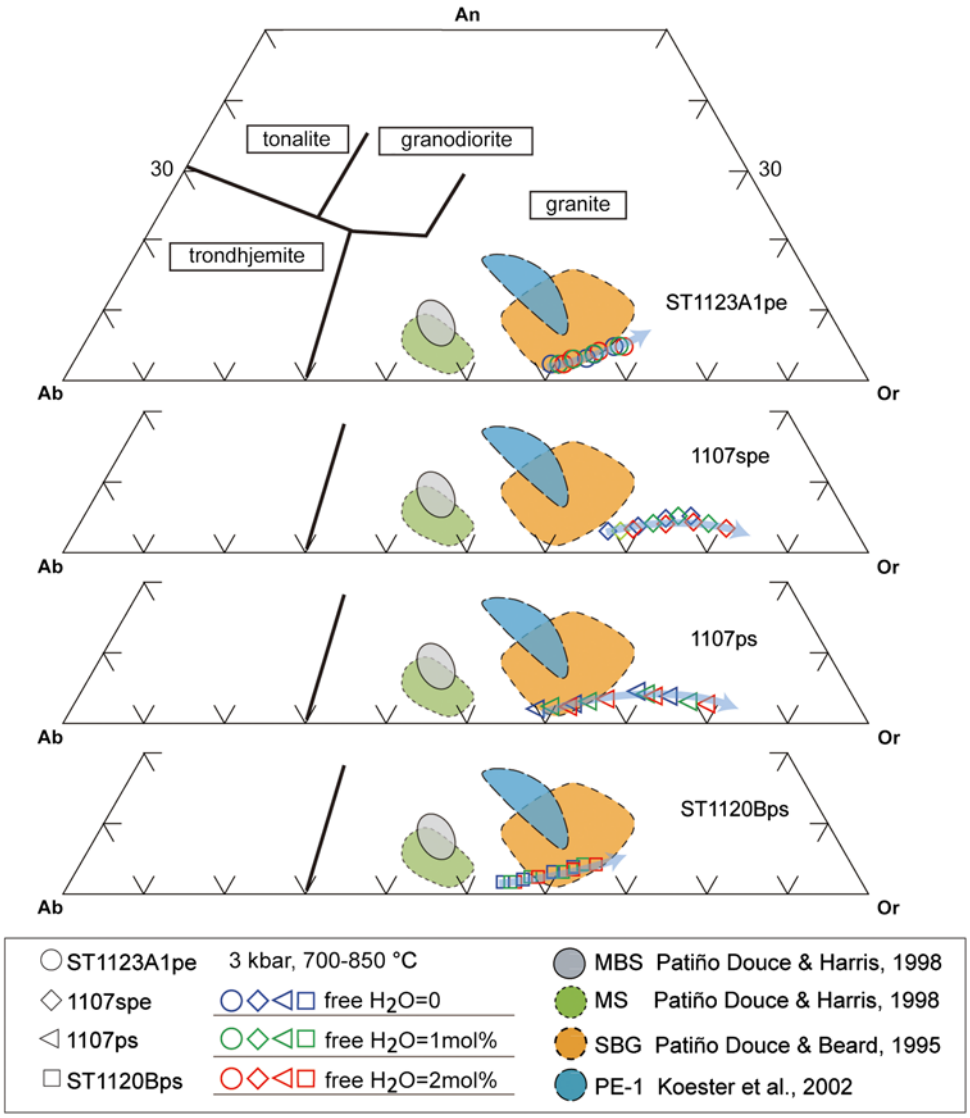

Fig. 12. (Colour online) Normative albite–anorthite–orthoclase (Ab–An–Or) contents of melt calculated at 3 kbar. Classification of silicic melts after Barker (1979). The experimental glass compositions are included for comparison (Patiño-Douce & Beard, 1995; Patiño-Douce & Harris, 1998; Koester *et al.* 2002). The melt compositions for different samples are represented by hollow circles (ST1123A1), diamonds (1107spe), triangles (1107ps) and squares (ST1120B), and the colours (blue, green and red) of the symbols are used for designating the water contents. The arrows show the direction of temperature increase.

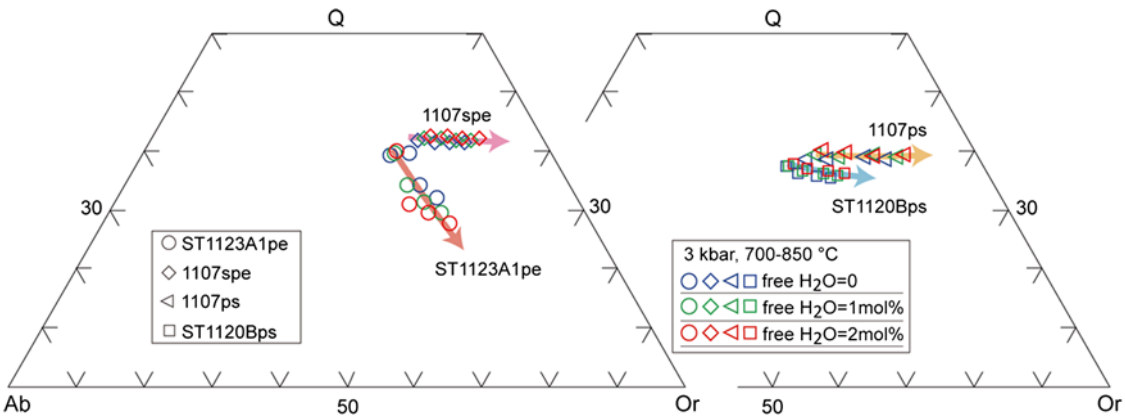

Fig. 13. (Colour online) CIPW normative proportions of quartz (Q), albite (Ab) and orthoclase (Or) for melt compositions at 3 kbar. The melt compositions for different samples are represented by hollow circles (ST1123A1), diamonds (1107spe), triangles (1107ps) and squares (ST1120B), and the colours (blue, green and red) of the symbols are used for designating the water contents. The arrows show the direction of temperature increase.

https://doi.org/10.1017/S001675681800078X Published online by Cambridge University Press

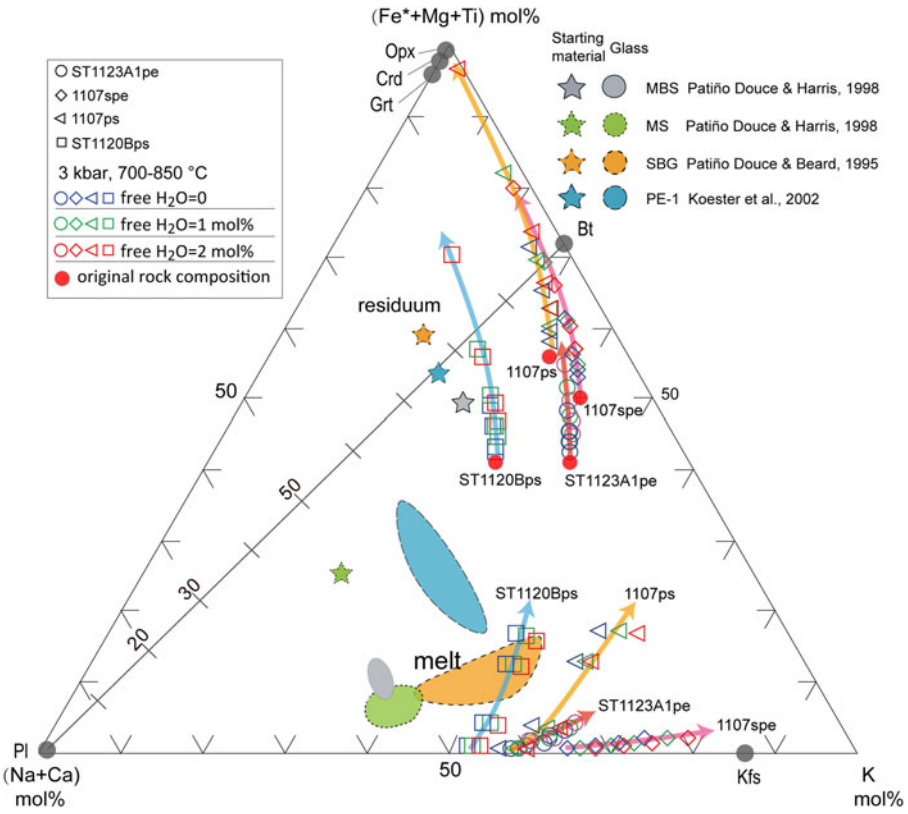

Fig. 14. (Colour online) Ternary (Na+Ca)–(Fe*+Mg+Ti)–K plot (after Solar & Brown, 2001; Brown *et al.* 2016) showing the melt and residuum evolution at varying water conditions. The experimental glass compositions were included for comparison (Patiño-Douce & Beard, 1995; Patiño-Douce & Harris, 1998; Koester *et al.* 2002). The melt and residuum compositions for different samples are represented by hollow circles (ST1123A1), diamonds (1107spe), triangles (1107ps) and squares (ST1120B), and the colours (blue, green and red) of the symbols are used for designating the water contents. The arrows show the direction of temperature increase. The red dots are the original rock compositions for modelling.

place crucial constraints on the protolith composition of granulites that occurred in a progressive metamorphic sequence comparable with those exposed at Mt Stafford.

8. Conclusions

The phase equilibrium modelling of pelitic, semi-pelitic and high- and low- ferromagnesian psammitic rocks at Mt Stafford quantitatively illustrates the dependence of the melt productivity and composition on rock composition and water content. Subtle variations in the proportion of free water content can result in appreciable changes in melt mode. At high-temperature zones close to the heat source, the pelitic and psammitic metasedimentary rocks possibly underwent rapid heating and retained various amounts of water to solidus. The potential discrepancy in water retained to super-solidus conditions may have contributed to the different melting histories of pelitic and psammitic rocks in the field. Melt composition depends strongly on protolith composition and, for a given protolith, added water does not significantly change melt composition. The modelling shows that by melt loss alone, normal sedimentary rocks can hardly produce the extremely high ferromagnesian and low alkali compositions of the melanosome/mesosome observed in the field. The special compositions of some melanosome/mesosome may be inherited mainly from their protoliths. The topologies of phase relationships in the *P*–*T* space, in the range of compositions investigated, are not very sensitive to composition changes. The major mineral assemblages of the metasedimentary rocks are not markedly affected by water activity. The major difference resulting from increasing initial water will basically be melt production, rather than the nature of the paragenesis. Consequently, neither the melting reaction nor the mineral paragenesis alone is a reliable indicator of the original water content of the rocks.

Supplementary material. To view supplementary material for this article, please visit https://doi.org/10.1017/S001675681800078X.

Acknowledgements. The programme was financially supported by ARC Discovery Project funding (DP160103449) NRD, the University of Sydney and Macquarie University, the National Natural Science Foundation of China (41672062, 41202047, 41502059), and the Fundamental Research Funds of CAGS(JYYWF201819). WW was supported by a University of Sydney International Postgraduate Award. This study used instrumentation funded by ARC LIEF and DEST Systemic Infrastructure Grants, Macquarie University and Industry. This is contribution XXX from the ARC Centre of Excellence for Core to Crust Fluid Systems (www.ccfs.mq.edu.au) and XXX from the GEMOC Key Centre (www.gemoc.mq.edu.au).

References

Acosta-Vigil A, London D, Morgan VI GB, Cesare B, Buick B, Hermann J and Bartoli O (2017) Primary crustal melt compositions: insights into the controls, mechanisms and timing of generation from kinetics experiments and melt inclusions. *Lithos* **286–287**, 454–79.

Barker FF (1979) Trondhjemites: definition, environment, and hypotheses of origin. In *Trondhjemites, Dacites and Related Rocks* (ed. FF Barker), pp. 1–12. Amsterdam: Elsevier.

Ben Othman D, Polvé M and Allègre CJ (1984) Nd–Sr isotopic composition of granulites and constraints on the evolution of the lower continental crust. *Nature* **307**, 510–5.

Bénard F, Moutou P and Pichavant M (1985) Phase relations of tourmaline leucogranites and the significance of tourmaline in silicic magmas. *Journal of Geology* **93**, 271–91.

Berger A, Burri T, Alt-Epping P and Engi M (2008) Tectonically controlled fluid flow and water-assisted melting in the middle crust: an example from the Central Alps. *Lithos* **102**, 598–615.

Blake DH and Page RW (1988) The Proterozoic Davenport province, central Australia: regional geology and geochronology. *Precambrian Research* **40–41**, 329–40.

Braun I, Raith M and Kumar GRR (1996) Dehydration-melting phenomena in leptynitic gneisses and the generation of leucogranites: a case study from the Kerala Khondalite Belt, southern India. *Journal of Petrology* **37**, 1285–305.

Brown M (1973) The definition of metatexis, diatexis and migmatite. *Proceedings of the Geologists' Association* **84**, 371–82.

Brown M (1994) The generation, segregation, ascent and emplacement of granite magma: the migmatite-to-crustally-derived granite connection in thickened orogens. *Earth-Science Reviews* **36**, 83–130.

Brown M (2001) Orogeny, migmatites and leucogranites: a review. *Proceedings of the Indian Academy of Science (Earth and Planetary Science)* **110**, 313–36.

Brown M (2010) The spatial and temporal patterning of the deep crust and implications for the process of melt extraction. *Philosophical Transactions of the Royal Society, Series A* **368**, 11–51.

Brown M (2013) Granite: from genesis to emplacement. *Geological Society of America Bulletin* **125**, 1079–113.

Brown M and Korhonen FJ (2009) Some remarks on melting and extreme metamorphism of crustal rocks. In *Physics and Chemistry of the Earth's Interior* (eds AK Gupta and S Dasgupta), pp. 67–87. New York: Indian National Science Academy, Springer (India) Private Limited.

Brown M, Rushmer T and Sawyer EW (1995) Introduction to special section: mechanisms and consequences of melt segregation from crustal protoliths. *Journal of Geophysical Research* **100**, 15551–63.

Brown CR, Yakymchuk C, Brown M, Fanning CM, Korhonen FJ, Piccoli PM and Siddoway CS (2016) From source to sink: petrogenesis of Cretaceous anatectic granites from the Fosdick migmatite–granite complex, West Antarctica. *Journal of Petrology* **57**, 1241–78.

Buick IS, Stevens G and Gibson RL (2004) The role of water retention in the anatexis of metapelites in the Bushveld Complex Aureole, South Africa: an experimental study. *Journal of Petrology* **45**, 1777–97.

Carvalho BB, Sawyer EW and Janasi VA (2016) Crustal reworking in a shear zone: transformation of metagranite to migmatite. *Journal of Metamorphic Geology* **34**, 237–64.

Chorlton LB and Martin RF (1978) The effect of boron on the granite solidus. *Canadian Mineralogist* **16**, 239–44.

Clarke GL, Collins WJ and Vernon RH (1990) Successive overprinting granulite facies metamorphic events in the Anmatjira Range, central Australia. *Journal of Metamorphic Geology* **8**, 65–88.

Clarke GL, Fitzherbert JA, Milan LA, Daczko NR and Degeling HS (2010) Anti-clockwise P-T paths in the lower crust: an example from a kyanite-bearing regional aureole, George Sound, New Zealand. *Journal of Metamorphic Geology* **28**, 77–96.

Clemens JD (2006) Melting of the continental crust: fluid regimes, melting reactions, and source-rock fertility. In *Evolution and Differentiation of the Continental Crust* (eds M Brown and T Rushmer), pp. 297–331. Cambridge: Cambridge University Press.

Clemens JD and Holness MB (2000) Textural evolution and partial melting of arkose in a contact aureole: a case study and implications. *Visual Geosciences* **5**, 1–14.

Clemens JD and Vielzeuf D (1987) Constraints on melting and magma production in the crust. *Earth and Planetary Science Letters* **86**, 287–306.

Coggon R and Holland TJB (2002) Mixing properties of phengitic micas and revised garnet-phengite thermobarometers. *Journal of Metamorphic Geology* **20**, 683–96.

Collins WJ and Vernon RH (1992) Palaeozoic arc growth, deformation and migration across the Lachlan Fold Belt, southeastern Australia. In *The Palaeozoic Eastern Margin of Gondwanaland: Tectonics of the Lachlan Fold Belt, Southeastern Australia and Related Orogens* (eds CL Fergusson and RA Glen). Tectonophysics **214**, 381–400.

Compston DM (1995) Time constraints on the evolution of the Tennant Creek Block, northern Australia. *Precambrian Research* **71**, 107–29.

Craven SJ, Daczko NR and Halpin JA (2012) Thermal gradient and timing of high-T–low-P metamorphism in the Wongwibinda Metamorphic Complex, southern New England Orogen, Australia. *Journal of Metamorphic Geology* **30**, 3–20.

Craven SJ, Daczko NR and Halpin JA (2013) High-T–low-P thermal anomalies superposed on biotite-grade rocks, Wongwibinda Metamorphic Complex, southern New England Orogen, Australia: heat advection by aqueous fluid? *Australian Journal of Earth Sciences* **60**, 621–35.

Droop GTR and Brodie KH (2012) Anatectic melt volumes in the thermal aureole of the Etive Complex, Scotland: the roles of fluid-present and fluid-absent melting. *Journal of Metamorphic Geology* **30**, 843–64.

Droop GTR, Clemens JD and Dalrymple DJ (2003) Processes and conditions during contact anatexis, melt escape and restite formation: the Huntly Gabbro complex, NE Scotland. *Journal of Petrology* **44**, 995–1029.

Etheridge MA, Wall VJ and Cox SF (1984) High fluid pressures during regional metamorphism and deformation: implications for mass transport and deformation mechanisms. *Journal of Geophysical Research* **89**, 4344–58.

Fyfe WS (1973) The granulite facies, partial melting and the Archean crust. *Philosophical Transactions of the Royal Society of London, Series A* **273**, 457–61.

Genier F, Bussy FO, Epard J-L and Baumgartner L (2008) Water-assisted migmatization of metagraywackes in a Variscan shear zone, Aiguilles-Rouges massif, western Alps. *Lithos* **102**, 575–97.

Grant JA (2009) THERMOCALC and experimental modelling of melting of pelite, Morton Pass, Wyoming. *Journal of Metamorphic Geology* **27**, 571–8.

Greenfield JE, Clarke GL, Bland M and Clark DC (1996) In-situ migmatite and hybrid diatexite at Mt Stafford, central Australia. *Journal of Metamorphic Geology* **14**, 413–26.

Greenfield JE, Clarke GL and White RW (1998) A sequence of partial melting reactions at Mt. Stafford, central Australia. *Journal of Metamorphic Geology* **16**, 363–78.

Guilmette C, Indares A and Hébert R (2011) High-pressure anatectic paragneisses from the Namche Barwa, Eastern Himalayan Syntaxis: textural evidence for partial melting, phase equilibria modeling and tectonic implications. *Lithos* **124**, 66–81.

Hanson RB and Barton MD (1989) Magmatism and the development of low-pressure metamorphic belts: implications from the western United States and thermal modelling. *Geological Society of America Bulletin* **101**, 1051–65.

Harte B, Hunter RH and Kinny PD (1993) Melt geometry, movement and crystallisation, in relation to mantle dykes, veins and metasomatism. *Philosophical Transactions of the Royal Society of London, Series A* **342**, 1–21.

Harte B, Pattison DRM and Linklater CM (1991) Field relations and petrography of partially melted pelitic and semi-pelitic rocks. In *Equilibrium and Kinetics in Contact Metamorphism, the Ballachulish Igneous Complex and its Aureole* (eds G Voll, J Töpel, DRM Pattison and F Seifert), pp. 182–210. Berlin: Springer.

Holland TJB and Powell R (1998) An internally consistent thermodynamic data set for phases of petrological interest. *Journal of Metamorphic Geology* **16**, 309–43.

Holland TJB and Powell R (2003) Activity–composition relations for phases in petrological calculations: an asymmetric multicomponent formulation. *Contributions to Mineralogy and Petrology* **145**, 492–501.

Holness MB, Cesare B and Sawyer EW (2011) Melted rocks under the microscope: microstructures and their interpretation. *Elements* **7**, 247–52.

Holness MB and Clemens JD (1999) Partial melting of the Appin Quartzite driven by fracture-controlled H_2O infiltration in the aureole of the Ballachulish Igneous Complex, Scottish Highlands. *Contributions to Mineralogy and Petrology* **136**, 154–68.

Holness MB and Sawyer EW (2008) On the pseudomorphing of melt-filled pores during the crystallization of migmatites. *Journal of Petrology* **49**, 1343–63.

Holtz F and Johannes W (1991) Genesis of peraluminous granites I: experimental investigation of melt compositions at 3 and 5 MPa and various H_2O activities. *Journal of Petrology* **32**, 935–58.

Johannes W and Holtz F (1990) Formation and composition of H_2O-undersaturated granitic melts. In *High-Temperature Metamorphism and Crustal Anatexis* (eds JR Ashworth and M Brown), pp. 87–104. London: Unwin Hyman.

Johannes W and Holtz F (1996) *Petrogenesis and Experimental Petrology of Granitic Rocks*. Berlin: Springer, 335 pp.

Johnson TE, Brown M and Solar GS (2003) Low-pressure subsolidus and suprasolidus phase equilibria in the MnNCKFMASH system: constraints

https://doi.org/10.1017/S001675681800078X Published online by Cambridge University Press

on conditions of regional metamorphism in western Maine, northern Appalachians. *American Mineralogist* **88**, 624–38.

Johnson TE, Hudson N and Droop G (2001) Melt segregation structures within the Inzie Head gneisses of the northeastern Dalradian. *Scottish Journal of Geology* **37**, 59–72.

Johnson TE, White RW and Brown M (2011) A year in the life of an aluminous metapelite xenolith–the role of heating rates, reaction overstep, H_2O retention and melt loss. *Lithos* **124**, 132–43.

Kalt A, Berger A and Blumel P (1999) Metamorphic evolution of cordierite-bearing migmatites from the Bayerische Wald (Variscan Belt, Germany). *Journal of Petrology* **40**, 601–27.

Kerrick DM (1991) Overview of contact metamorphism. *Reviews in Mineralogy and Geochemistry* **26**, 1–12.

Koester E, Pawley AR, Fernandes LAD, Porcher CC and Soiani E (2002) Experimental melting of cordierite gneiss and the petrogenesis of syntranscurrent peraluminous granites in southern Brazil. *Journal of Petrology* **43**, 1595–616.

Laporte D, Rapa Ille C and Provost A (1997) Wetting angles, equilibrium melt geometry, and the permeability threshold of partially molten crustal protoliths. In *Granite: From Segregation of Melt to Emplacement Fabrics* (eds JL Bouchez, DHW Hutton and WE Stephens), pp. 31–54. Dordrecht: Kluwer.

Le Breton N and Thompson AB (1988) Fluid-absent (dehydration) melting of biotite in metapelites in the early stages of crustal anatexis. *Contributions to Mineralogy and Petrology* **99**, 226–37.

Marchildon N and Brown M (2002) Grain-scale melt distribution in two contact aureole rocks: implications for controls on melt localisation and deformation. *Journal of Metamorphic Geology* **20**, 381–96.

McKenzie D (1984) The generation and compaction of partially molten rock. *Journal of Petrology* **25**, 713–65.

Mehnert KR (1968) *Migmatites and the Origin of Granitic Rocks*. Amsterdam: Elsevier, 393 pp.

Noakes LC (1953) The structure of the Northern Territory with relation to mineralization. In *Geology of Australian Ore Deposits. Fifth Empire Mining and Metallurgical Congress, Australia and New Zealand* (ed. AB Edwards), pp. 284–96. Melbourne: Australasian Institute of Mining and Metallurgy.

Patiño-Douce AE (1996) Effects of pressure and H_2O content on the compositions of primary crustal melts. *Transactions of the Royal Society of Edinburgh: Earth Sciences* **87**, 11–21.

Patiño-Douce AE and Beard JS (1995) Dehydration-melting of biotite gneiss and quartz amphibolite from 3 to 15 kbar. *Journal of Petrology* **36**, 707–38.

Patiño-Douce AE and Harris NBW (1998) Experimental constraints on Himalayan anatexis. *Journal of Petrology* **39**, 689–710.

Patiño-Douce AE and Johnson AD (1991) Phase equilibria and melt productivity in the pelitic system: implication for the origin of peraluminous granitoids and aluminous granulites. *Contributions to Mineralogy and Petrology* **107**, 202–18.

Patiño-Douce AE and McCarthy TC (1998) Melting of crustal rocks during continental collision and subduction. In *When Continents Collide: Geodynamics and Geochemistry of Ultrahigh-Pressure Rocks* (eds BR Hacker and JG Liou), pp. 27–55. Dordrecht: Kluwer.

Pattison DRM and Harte B (1988) Evolution of structurally contrasting anatectic migmatites in the 3-kbar Ballachulish aureole, Scotland. *Journal of Metamorphic Geology* **6**, 475–94.

Pichavant M (1981) An experimental study of the effect of boron on a water saturated haplogranite at 1 kbar vapour pressure. *Contributions to Mineralogy and Petrology* **76**, 430–9.

Powell R (1983) Processes in granulite-facies metamorphism. In *Migmatites, Melting and Metamorphism* (eds MP Atherton and CD Gribble), pp. 127–39. Nantwich, Cheshire: Shiva.

Powell R, Holland TJB and Worley B (1998) Calculating phase diagram involving solid solutions via no-linear equations, with examples using THERMOCALC. *Journal of Metamorphic Geology* **16**, 577–86.

Puziewicz J and Johannes W (1988) Phase equilibria and compositions of Fe–Mg–Al minerals and melts in water-saturated peraluminous granitic systems. *Contributions to Mineralogy and Petrology* **100**, 156–68.

Rabinowicz M and Vigneresse JÄ (2004) Melt segregation under compaction and shear channeling: application to granitic magma segregation in a continental crust. *Journal of Geophysical Research: Solid Earth* **109**, 1978–2012.

Redler C,White RW and Johnson TE (2013) Migmatites in the Ivrea Zone (NW Italy): constraints on partial melting and melt loss in metasedimentary rocks from Val Strona di Omegna. *Lithos* **175–176**, 40–53.

Reichardt H and Weinberg RF (2012) Hornblende chemistry in meta- and diatexites and its retention in the source of leucogranites: an example from the Karakoram Shear Zone, NW India. *Journal of Petrology* **53**, 1287–318.

Rigby MJ, Droop GTR and Bromiley GD (2008) Variations in fluid activity across the Etive thermal aureole, Scotland: evidence from cordierite volatile contents. *Journal of Metamorphic Geology* **26**, 331–46.

Rosenberg CL and Handy MR (2005) Experimental deformation of partially melted granite revisited: implications for the continental crust. *Journal of Metamorphic Geology* **23**, 19–28.

Rosenberg CL and Riller U (2000) Partial melt topology in statically and dynamically recrystallised granite. *Geology* **28**, 7–10.

Rubatto D, Hermann J and Buick IS (2006) Temperature and bulk composition control on the growth of monazite and zircon during low-pressure anatexis (Mount Stafford, central Australia). *Journal of Petrology* **47**, 1973–96.

Sawyer EW (2010) Migmatites formed by water-fluxed partial melting of a leucogranodiorite protolith: microstructures in the residual rocks and source of the fluid. *Lithos* **116**, 273–86.

Scrimgeour I, Smith JB and Raith JG (2001) Palaeoproterozoic high-T, low-P metamorphism and dehydration melting in metapelites from the Mopunga Range, Arunta Inlier, central Australia. *Journal of Metamorphic Geology* **19**, 739–57.

Skjerlie KP and Johnston AD (1992) Vapor-absent melting at 10 kbar of a biotite- and amphibole-bearing tonalitic gneiss: implications for the generation of A-type granites. *Geology* **20**, 263–6.

Skjerlie KP, Patiño-Douce AE and Johnston AD (1993) Fluid absent melting of a layered crustal protolith: implications for the generation of anatectic granites. *Contributions to Mineralogy and Petrology* **114**, 365–78.

Slagstad T, Jamieson RA and Culshaw NG (2005) Formation, crystallization, and migration of melt in the mid-orogenic crust: Muskoka domain migmatites, Grenville Province, Ontario. *Journal of Petrology* **46**, 893–919.

Solar GS and Brown M (2001) Petrogenesis of migmatites in Maine, USA. Possible source of peraluminous granite in plutons. *Journal of Petrology* **42**, 789–823.

Stevens G, Clemens JD and Droop GTR (1997) Melt production during granulite-facies anatexis: experimental data from "primitive" metasedimentary protoliths. *Contributions to Mineralogy and Petrology* **128**, 352–70.

Stewart AJ (1981) *Reynolds Range Region, Northern Territory, 1:100 000 Geological Map Commentary*. Canberra, ACT: Bureau of Mineral Resources, Geology and Geophysics, 22 pp.

Stewart AJ, Shaw RD and Black LP (1984) The Arunta Inlier: a complex ensialic mobile belt in central Australia. Part 1: stratigraphy, correlations and origin. *Australian Journal of Earth Sciences* **31**, 445–55.

Stuart CA, Daczko NR and Piazolo S (2017) Local partial melting of the lower crust triggered by hydration through melt–rock interaction: an example from Fiordland, New Zealand. *Journal of Metamorphic Geology* **35**, 213–30.

Stuart CA, Piazolo S and Daczko NR (2016) Mass transfer in the lower crust: evidence for incipient melt assisted flow along grain boundaries in the deep arc granulites of Fiordland, New Zealand. *Geochemistry, Geophysics, Geosystems* **17**, 3733–53.

Thompson AB (1982) Dehydration melting of pelitic rocks and the generation of H_2O-undersaturated granitic liquids. *American Journal of Science* **282**, 1567–95.

Thompson AB and Connolly JAD (1995) Melting of the continental crust: some thermal and petrological constraints on anatexis in continental collision zones and other tectonic settings. *Journal of Geophysical Research* **100**, 15565–79.

Tuttle OF and Bowen NL (1958) *Origin of Granite in the Light of Experimental Studies in the System $NaA1Si_3O_8$–$KA1Si_3O_8$–SiO_2–H_2O*. Geological Society of America Memoir no. 74.

Vernon RH, Clarke GL and Collins WJ (1990) Local, mid-crustal granulite facies metamorphism and melting: an example in the Mount Stafford area, central Australia. In *High Temperature Metamorphism and Crustal*

https://doi.org/10.1017/S001675681800078X Published online by Cambridge University Press

Anatexis (eds JR Ashworth and M Brown), pp. 272–319. London: Unwin Hyman.

Vielzeuf D and Holloway JR (1988) Experimental determination of the fluid-absent melting relations in the pelitic system. *Contributions to Mineralogy and Petrology* **98**, 257–76.

Vielzeuf D and Montel JM (1994) Partial melting of metagreywackes. Part I. Fluid-absent experiments and phase relationships. *Contributions to Mineralogy and Petrology* **117**, 375–93.

Vry J, Compston W and Cartwright I (1996) SHRIMP II dating of zircons and monazites: reassessing the timing of high-grade metamorphism and fluid flow in the Reynolds Range, northern Arunta Block, Australia. *Journal of Metamorphic Geology* **14**, 335–50.

Walte NP, Bons PD and Passchier CW (2005) Deformation of melt-bearing systems – insight from in situ grain-scale analogue experiments. *Journal of Structural Geology* **27**, 1666–79.

Wang W, Dunkley E, Clarke GL and Daczko NR (2014a) The evolution of zircon during low-P partial melting of metapelitic rocks: theoretical predictions and a case study from Mt Stafford, central Australia. *Journal of Metamorphic Geology* **32**, 791–808.

Wang W, Liu XS, Hu JM, Li ZH, Zhao Y, Zhai MG, Liu XC, Clarke GL, Zhang SH and Qu HJ (2014b) Late Paleoproterozoic medium-P high grade metamorphism of basement rocks beneath the northern margin of the Ordos Basin, NW China: petrology, phase equilibrium modelling and U–Pb geochronology. *Precambrian Research* **251**, 181–96.

Ward R, Stevens G and Kisters A (2008) Fluid and deformation induced partial melting and melt volumes in low-temperature granulite-facies metasediments, Damara Belt, Namibia. *Lithos* **105**, 253–71.

Warren RG (1983) Metamorphic and tectonic evolution of granulites, Arunta Block, central Australia. *Nature* **305**, 300–3.

Weinberg RF and Hasalová P (2015) Water-fluxed melting of the continental crust: a review. *Lithos* **212–215**, 158–88.

Wells PRA (1981) Accretion of continental crust: thermal and geochemical consequences. *Philosophical Transactions of the Royal Society of London, Series A* **301**, 347–57.

White AJR, Chappell BW and Cleaty JR (1974) Geologic setting and emplacement of some Australian Paleozoic batholiths and implications for intrusion mechanisms. *Pacific Geology* **8**, 159–71.

White RW, Pomroy NE and Powell R (2005) An in-situ metatexite-diatexite transition in upper amphibolite facies rocks from Broken Hill, Australia. *Journal of Metamorphic Geology* **23**, 579–602.

White RW and Powell R (2002) Melt loss and the preservation of granulite facies mineral assemblages. *Journal of Metamorphic Geology* **20**, 621–32.

White RW, Powell R and Clarke GL (2002) The interpretation of reaction textures in Fe-rich metapelitic granulites of the Musgrave Block, central Australia: constraints from mineral equilibria calculations in the system K_2O–FeO–MgO–Al_2O_3– SiO_2–H_2O–TiO_2–Fe_2O_3. *Journal of Metamorphic Geology* **20**, 41–55.

White RW, Powell R and Clarke GL (2003) Prograde metamorphic assemblage evolution during partial melting of metasedimentary rocks at low pressures: migmatites from Mt Stafford, central Australia. *Journal of Petrology* **44**, 1931–60.

White RW, Powell R and Holland TJW (2001) Calculation of partial melting equilibria in the system Na_2O–CaO–K_2O–FeO–MgO–Al_2O_3–SiO_2–H_2O (NCKFMASH). *Journal of Metamorphic Geology* **19**, 139–53.

White RW, Powell R and Holland TJB (2007) Progress relating to calculation of partial melting equilibria for metapelites. *Journal of Metamorphic Geology* **25**, 511–27.

White RW, Powell R, Holland TJB and Worley BA (2000) The effect of TiO_2 and Fe_2O_3 on metapelitic assemblages at greenschist and amphibolite facies conditions: mineral equilibria calculations in the system K_2O–FeO–MgO–Al_2O_3–SiO_2–H_2O–TiO_2–Fe_2O_3. *Journal of Metamorphic Geology* **18**, 497–511.

White RW, Stevens G and Johnson TE (2011) Is the crucible reproducible? Reconciling melting experiments with thermodynamic calculations. *Elements* **7**, 241–6.

Wickham SM (1987) Crustal anatexis and granite petrogenesis during low-pressure regional metamorphism–the Trois Seigneurs Massif, Pyrenees, France. *Journal of Petrology* **28**, 127–69.

Yakymchuk C and Brown M (2014) Consequences of open-system melting in tectonics. *Journal of the Geological Society, London* **171**, 21–40.

Yardley BWD (2009) The role of water in the evolution of the continental crust. *Journal of the Geological Society, London* **166**, 585–600.

Yardley BWD and Barber JP (1991) Melting reactions in the Connemara schists – the role of water infiltration in the formation of amphibolite facies migmatites. *American Mineralogist* **76**, 848–56.

Yardley BWD and Valley JW (1997) The petrologic case for a dry lower crust. *Journal of Geophysical Research* **102**, 12173–85.

Yardley BWD and Valley JW (2000) Comment on "The petrologic case for a dry lower crust" by Yardley, B. W. D. & Valley, J. W. – Reply. *Journal of Geophysical Research* **105**, 6065–8.

https://doi.org/10.1017/S001675681800078X Published online by Cambridge University Press